Development of a fabric-based surface-enhanced Raman spectroscopy (SERS) sensor for rapid detection of human disease biomarkers

By

Ashley Megan Robinson

A Thesis Submitted to
Saint Mary's University, Halifax, Nova Scotia
in Partial Fulfillment of the Requirements for
the Degree of Bachelor of Science, Honours in Chemistry

April 2014, Halifax, Nova Scotia

Approved : Dr. Christa Brosseau
Supervisor

Approved: Prof. Mary Sheppard
Examiner

Approved: Dr. Marc Lamoureux
Examiner

Date: April 25, 2014

Certification

Development of a fabric-based surface-enhanced Raman spectroscopy (SERS) sensor for rapid detection of human disease biomarkers

I hereby certify that this thesis was completed by Ashley Megan Robinson in partial fulfillment for the requirements of the Degree of Bachelor of Science with Honors in Chemistry at Saint Mary's University and I certify that this is truly the original work carried out by Ashley Megan Robinson.

Thesis Supervisor

Dr. Christa Brosseau

Chairperson of the Chemistry Department

Dr. Jason Masuda

Dean of Science

Dr. Steven M. Smith

ABSTRACT

Development of a fabric-based surface-enhanced Raman spectroscopy (SERS) sensor for rapid detection of human disease biomarkers

By Ashley Robinson

Currently, there is a growing demand for continuous monitoring of human disease and the development of analytical techniques capable of reliably detecting and diagnosing various illnesses. The objective of this project was the development of inexpensive, sensitive, and reproducible substrates for surface-enhanced Raman spectroscopy (SERS), from metal-coated silk fabric. Potentially, these substrates could be incorporated into clothing and other textiles for regular monitoring of biomarkers in bodily fluids or air pollutants. The main focus of this work was the roughening of the fabric samples on the nanoscale, which is a required feature of SERS substrates. This was achieved through electrochemical methods and the deposition of nanoparticles. All synthesized nanoparticles were characterized by transmission electron microscopy and ultraviolet-visible spectroscopy. The substrates were characterized by scanning electron microscopy, as well as by the SERS signal of 4,4'-bipyridine (4,4'-byp) collected on their surface. It was found that *in situ* synthesis of silver colloids on the fabric was most effective method for obtaining reliable and sensitive substrates, and the incubation of the fabric in gold nanoflowers provided a uniform and reproducible SERS substrate. The detection of 4,4'-byp on these surfaces was achieved with ease, whereas the biomolecules 2'-deoxyguanosine 5'-monophosphate, and guanosine could not be detected. A single band for guanine was identified in the SERS spectrum collected on a fabric substrate. Interference from the silk fibers, citrate and other reagents used in the synthesis of nanoparticles was identified as a key obstacle in the fabrication of fabric substrates for the detection of biomolecules by SERS.

April 25, 2014

Acknowledgements

I would like to thank my supervisor Dr. Christa L. Brosseau for having greatly enriched my undergraduate experience by guiding me through my Honours project and teaching me that patience, perspective and creativity are important aspects of research. Also, I would like to thank my group members: Osai Clarke, Reem Karaballi, Scott Harroun, Soraya Merchant and Mohammed Abul Hasanat, for their support and making the long hours in the lab all the more enjoyable. I am particularly thankful to Marwa Yasmin and Lili Zhao, who helped guide and assist me with this project. Additionally, I would like to acknowledge Achira Labs, in Bangalore, India, for supplying the fibers and fabrics, which constituted the foundation of my work, as well as Xiang Yang and Patricia Scallion for their assistance with imaging the fabric samples.

Moreover, I would like to express my gratitude to the faculty and staff of the Department of Chemistry, who have provided me with a solid foundation in Chemistry, as well as inspired me to challenge myself academically and aspire to greater achievements. Lastly, I would like to thank my family and friends for their continuous support.

Table of Contents Page

Table of Contents Continued Page

Table of Contents Continued Page

List of Figures

List of Figures Continued

List of Figures Continued

List of Figures Continued

Page

List of Tables Page

List of Abbreviations

4,4'-Byp	4,4'-Bipyridine
AgNPs	Silver nanoparticles
AuNFs	Gold nanoflowers
AuNPs	Gold nanoparticles
CE	Counter electrode
dGMP	2'-Deoxyguanosine 5'-monophosphate
EDX	Energy dispersive X-ray analysis
EM	Electron microscopy
LSPR	Localized surface plasmon
ORC	Oxidation-reduction cycle
PDDA	Poly(diallyldimethylammonium chloride)
RE	Reference electrode
SEM	Scanning electron microscope
SERS	Surface enhanced Raman spectroscopy
TEM	Transmission electron microscope
TOC	Truncated octahedral nanoparticles
WE	Working electrode

Chapter 1: Introduction

1.1 Preamble

For most analytical techniques, the ultimate goal is to improve sensitivity, guarantee reproducibility, and optimize the overall process by simplifying sample preparation and measurement procedures [1]. Ideally, analysis should also be well suited for widespread usage, which entails affordable testing and long-term durability of the instrumentation. In recent decades, there has been a particular focus on the development of analytical techniques for the detection, diagnosis and monitoring of human disease. Many advances have been made in this regard, however they have not all been made available to developing countries due to a lack of resources. A need persists for low-cost, simple to use, and rapid tests [2].

Of increasing interest is the application of spectroscopic approaches based on Raman scattering. In particular, the applications of surface-enhanced Raman spectroscopy (SERS) have been expanded to biosensing, due to its high sensitivity and selectivity [3], simple sample preparation, non-destructive nature, and rapid sensing [4]. This technique is highly dependent on the distribution of molecules on a SERS substrate, which is a complicated system; both the uniformity of the metal surface on the nanoscale and the orientation of molecules on the surface impact the SERS signal [1]. For this reason, the optimization of SERS substrates for the detection of a wide variety of biomolecules is of particular focus. It must be noted that the main difficulty associated with inexpensive SERS substrate fabrication is non-uniformity. Many techniques that are capable of producing uniform SERS substrates with good enhancement factors, such as electron beam lithography, are very expensive, time consuming, and produce small

surface areas [5].

1.2 Objective of this Thesis

The objective of this work was to develop sensitive, reproducible, and cost-effective SERS substrates from metal-coated silk fabric. The metal-coated fabric was manufactured in India on a large scale and at low cost. The nature of this substrate would facilitate its incorporation into clothing and other textiles. This technology therefore presents the opportunity for rapid monitoring of disease biomarkers found in bodily fluids (i.e. sweat or urine) or evaluating exposure to air pollutants. By modifying the fabric samples through electrochemical methods and deposition of nanoparticles, the detection of 4,4'-bipyridine (4,4'-byp) was made possible. 4,4'-Byp is a strong Raman scatterer, therefore an attempt at detecting weak Raman scatterers, such as biomolecules, was also explored.

1.3 Scope of this Thesis

This thesis consists of five chapters. Chapter 1 provides a context for this project, and outlines the objectives of this work. Chapter 2 presents a literature review of the important elements of the work, as well as any background theory pertaining to the instrumentation and techniques applied, such as Raman spectroscopy, electron microscopy, and electrochemistry. Chapter 3 summarises the experimental procedures of this thesis, including electrochemical methods and nanoparticle syntheses.

The major experimental results are provided in Chapter 4. These include the outcomes of electrochemical roughening, the characterization of nanoparticles, as well as the SERS of analytes on these substrates. Chapter 5 outlines the main results obtained

from this body of work, and proposes new directions that may be pursued in the future.

Chapter 2: Background

2.1 Fabric-Based Sensors

In recent years, NASA has focused on the development of "Smart Fabrics", which are traditional fabrics, such as cotton and polyester, with integrated active functionalities. These functionalities include biomedical sensing devices, power generation and storage, or assistive technology [6]. Smart Fabrics can be made up of conductive or semi-conductive threads and yarns, modified by nanoelectronics, or chemically treated to provide different features [6]. These fabrics are aimed for specific uses, however the widespread production of wearable sensors is also in high demand within the medical sector. Continuous monitoring technology could aid physicians to assess patient health data, and help diagnose diseases that are generally detected with difficulty without close monitoring [7]. For example, people suffering from Parkinson's disease could greatly benefit from objective recordings by wearable sensors that would provide data concerning freezing of gait and nighttime disability, two events that cannot be collected during a clinical visit [8].

Wearable sensors have been developed, and are often made from conductive fabric materials [9]. Liu *et al*. [10] have shown that the incorporation of conductive yarns into undergarments can create intelligent incontinence pants, which can monitor, sense and alert the wearer and care provider on the incontinence status, to reduce the need for frequent manual checking. Textiles are ideal for the design of wearable biosensors; they are flexible, soft, strong, and light. These favorable properties allow them to be constantly worn without affecting an individual's daily routine [11]. The physical and chemical properties of textiles allow these materials to act as matrixes, by immobilizing

and adsorbing various substances [11, 12]. However, most wearable sensors are focused on physiological monitoring, while very few focus on obtaining chemical information residing on the skin or in the bodily fluids of the wearer, which could provide further insight into overall health [12, 13]. For example, the continuous monitoring of biomarkers for oxidative stress, a condition related to numerous diseases, such as cancer, sepsis, and epilepsy [14], could ease diagnosis. Nevertheless, work by Lee *et al*. [15] demonstrates how aptamer-conjugated gold nanoparticles (AuNPs) can be used for protein analysis on fabric pads, via colorimetric biosensing, as a model for point-of-care diagnosis. Additionally, chemical analysis on wearable textiles has been pursued, for the evaluation of toxins in the environment. Chuang *et al*. [16] have shown that screen-printed electrodes on GORE-TEX® fabric can be used to detect nitroaromatic explosives, which is suitable for the development of monitoring systems integrated into conventional clothing for soldiers or security personnel.

2.2 Raman Spectroscopy

Raman spectroscopy is an analytical technique based on the scattering of monochromatic light as it interacts with a sample. Raman and Krishnan discovered this technique in 1928 [4]. In a typical experiment, the sample of interest is illuminated with a laser beam at a power ranging from 50–400 mW [17]. When the beam is focused on a sample, a portion of the light passes through the sample and remains unchanged, while a small fraction, approximately 0.1%, is elastically scattered, maintaining the same frequency as the incident light [4]. This type of scattering is termed Rayleigh scattering, and does not contribute to the Raman signal. Inelastic scattering is what leads to the formation of a vibrational profile of a given molecule. This scattering effect is relatively

low because only one in about 10^6 incident photons will be Raman scattered [4]. As depicted in Figure 1, these photons may be Stokes or anti-Stokes scattered, indicating that they experience a net energy loss or gain, respectively, after interaction with a sample [18]. Stokes scattering is more likely than anti-Stokes, because most molecules are excited to a virtual state from the electronic ground state, rather than excited from an initial vibrational state [19]. The Raman spectrum is generally observed in the ultraviolet–visible (UV-vis) portion of the electromagnetic spectrum [4].

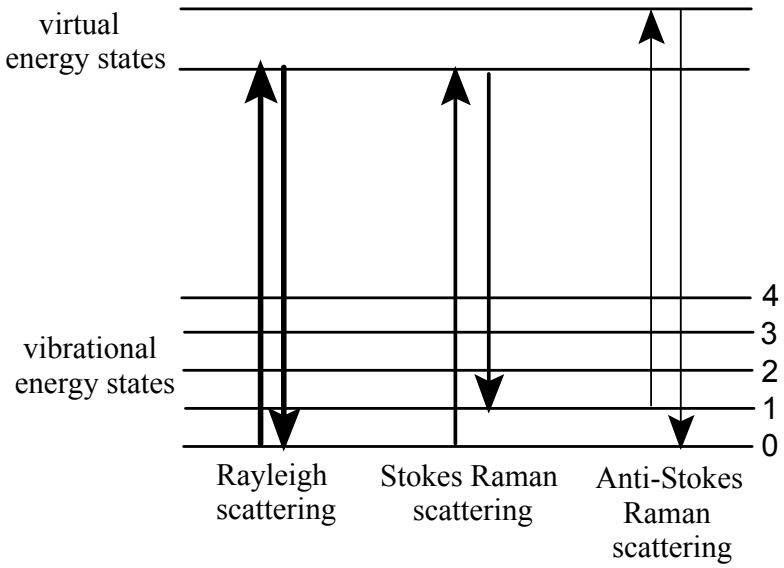

Figure 1. Various types of scattering that may occur when monochromatic light interacts with a sample: Rayleigh, Stokes, and anti-Stokes.

Raman spectroscopy possesses key strengths over other forms of vibrational spectroscopy, such as infrared spectroscopy, to which it is complimentary [20]. This method is rapid, non-destructive, and does not require the sample to be transparent [4], nor free of water, because water is a weak Raman scatterer. Raman spectroscopy is therefore an ideal tool for the analysis of various biological samples, which usually contain above 50% water [20]. This technique however, is not ideal for the analysis of

samples that exhibit strong fluorescence, which can overwhelm the weak Raman signal. This problem may be resolved by using near-infrared excitation, thereby avoiding the electronic absorption bands of most fluorescent species, and thus preventing their excitation [17]. Another limitation of Raman spectroscopy is that it has low sensitivity, because Raman scattering is a weak effect. This means that samples must be present at high concentrations for this method of analysis to be effective.

2.3 Surface-Enhanced Raman Spectroscopy

Surface enhanced Raman spectroscopy (SERS) is a technique that overcomes many limitations of normal Raman spectroscopy. It was discovered in 1974, when Fleischmann *et al.* [21] observed an increase in the Raman signal of pyridine when it was absorbed onto a roughened silver electrode surface. Although the unusually intense Raman signals were initially attributed to high surface concentration due to electrochemical roughening, it is now understood that the increase in scattering intensity is due to surface properties of the roughened metal substrate [22, 23]. The two most widely accepted mechanisms proposed to account for the experimental results of SERS are the electromagnetic enhancement and chemical enhancement mechanisms [22, 23, 24]. In order for electromagnetic enhancement to occur, the metal surface must be carefully designed and roughened on the nanoscale. Nanofeatures can be tuned to exhibit surface plasmons that amplify both the incident laser field and the inelastically scattered field [25]. A localized surface plasmon resonance (LSPR) arises when the collective oscillation of valence electrons in a metal nanoparticle is in resonance with the frequency of the incident light, as shown in Figure 2 [24].

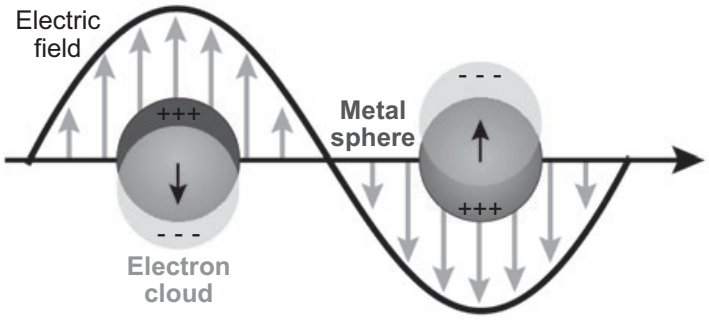

Figure 2. Illustration of the localized surface plasmon. Reproduced with permission [24].

An electromagnetic wave acting on a metal surface has a penetration depth of only ~50 nm for silver and gold [26], which is why the LSPR concerns only electrons at the surface. Additionally, the collective oscillation of free electrons is confined to a finite volume, defined by the particle dimensions [26]. It is the amplification of both the incident laser field and the scattered Raman field through their interaction with the surface when a surface plasmon is present that causes the Raman signal to be enhanced [23].

The chemical enhancement mechanism is related to the interactions between the metal and adsorbed molecule. It has been hypothesized that the electronic states of the adsorbate are shifted by their interaction with the metal, although more evidence exists that new electronic states arise from chemisorption and serve as resonant intermediate states [23]. Collectively, the two mechanisms outlined above enhance the Raman signal by factors of up to 10^6-10^7 [27]. Overall, the enhancement provided by SERS allows the collection of spectra from samples in parts per billion concentration [25], making it an ideal method of analysis for biological samples, in which analytes are typically found in trace quantities.

In addition to high sensitivity and simultaneous detection of multiple compounds [28], SERS possesses all the same advantages as normal Raman spectroscopy compared to other analytical techniques. SERS is a distance-dependent method: the analyte must be within a few nanometers of the surface to be detected [22]. This dependence greatly affects the SERS signals of analytes. It has been illustrated in work by Podstawka-Proniewicz *et al*. [29], that the interaction of a biomolecule, neuromedin C, with different electrochemically roughened metal substrates alters the SERS signal. Differences arise in the spectra, depending on how close certain functional groups are to the substrate. This property allows SERS to be used to evaluate inter- or intra-molecular interactions, as well as different conformational states [27].

A major hurdle associated with SERS is a lack of signal reproducibility that arises from non-uniform plasmonic field enhancement, which is directly related to the morphology of the nanostructured metal substrates [30]. The design of SERS substrates with uniform enhancement is therefore key to establishing this technique as a detection method for biomolecules.

2.4 SERS Substrates

The wide-variety of metallic substrates that exist today allow SERS experiments to be tuned appropriately for the detection or monitoring of a given analyte. These include lithographically produced nanostructures, and the preparation of metal-island films on solid surfaces by sputter coating, mechanical polishing, and vapour-deposition [31]. It must be recognized however, that electrochemically roughened electrode surfaces and metal colloids are the most commonly used SERS substrates [32, 22]. Generally, metals with high optical reflectivity, such as silver, gold or copper are used as SERS

substrates, although copper is rarely used, due to its chemical instability and weaker SERS activity. This said, copper is propitious from the perspective that chemisorption of various types of organic compounds is favoured on this metal, and it is less expensive than its counterparts [33].

Noble metal electrodes have been shown to have reproducible surface roughness when generated by electrochemical oxidation-reduction cycles (ORCs) [31, 34]. Aqueous potassium chloride solutions are most commonly used for this process, although various sulfate solutions may also be employed [31]. More recently, electrochemical roughening has been shown to be the simplest way of obtaining SERS-active transition metal surfaces [35].

In the case of colloids, silver and gold nanoparticles ranging from 10-100 nm in diameter are most commonly used for SERS studies [36]. These can be used directly as a colloidal suspension or allowed to dry on a surface. Nanoparticles can be prepared by laser ablation, but are more commonly synthesized by different *in situ* reduction processes [36]. Improved SERS signals (i.e. with greater enhancement factors, stability and reproducibility) have been achieved through the synthesis of variously shaped colloids [20]. These include spheres, rods, cubes, triangles, and shells [5]. The synthesis of nanostars in particular, has been largely investigated for applications in SERS, because it is predicted that focalization of the plasmonic electromagnetic field at the tips of the nanostars provides significant enhancement in comparison to spherical nanoparticles [37]. Nanostars may be prepared by a seeded-growth technique, which usually leads to monodisperse particles, or by one-pot methods, which typically lead to a wider distribution of particle size and shape [37]. Typically, the synthesis of these well-defined

nanostructures involves the use of surfactants, which are highly undesirable for SERS applications because they cause signal interference due to strong surface adsorption. Nevertheless, surfactant-free syntheses do exist, as reported by Jena *et al*. [38] who described a nontoxic and environmentally safe preparation of silver nanoparticles (AgNPs), with a flowerlike morphology that is not contaminated by surfactants. Furthermore, alternative methods for preparing SERS-active substrates, as shown by Scholes *et al*. [39], involve depositing SERS-active nanoparticles on micro-structured surfaces. These substrates are reported to provide an increase in the observed signal intensities, compared to those achieved on either nanoparticles alone, or the micro-structured surface.

An additional aspect influencing the development of substrates for the detection of biomolecules is the minimization of production costs, because high throughput manufacturing would facilitate the transition from research laboratories to real-world application [30]. For this reason, many paper-based sensors have been explored. High packing density and uniform distribution of metal nanoparticles in solution can be easily transferred to paper, because the water is quickly drawn up by the substrate [40]. Similarly, Chakraborty *et al.* [41] have shown that Ag_{152} clusters can be coated uniformly on paper, cotton and silk. Work by Figueroa [42] showed that printable silver nanoparticle ink could be deposited on papers and polymers to detect hyaluronic acid, a biomarker for the early detection of liver disease found in human serum, using SERS. The development of a uniform, inexpensive SERS-active substrate that would provide significant signal enhancement is in high demand for the monitoring of various biological conditions.

2.5 SERS on Fabric Substrates

Currently, there exists only a dozen or so publications concerning the use of textiles and fabric as SERS substrates. For this reason, this is an area of research with great potential for development and exploration. Of the few SERS studies performed on fabric, Kim *et al*. [43] have shown that it is possible to use cotton fabrics to observe the exchange reaction between benzenethiol and 4-nitrobenzenethiol. In other studies, the SERS spectrum of alizarin dye on silk treated with silver nanoparticles was collected [44], and the crystallinity of silicon films on woven polyester was assessed by SERS [45]. It is evident that no such work has yet employed fabric as a SERS substrate for its specific properties, i.e. its flexibility and strength, allowing straightforward incorporation into other textiles, as is attempted in this work.

2.6 Electrochemistry

Electrochemistry is a branch of chemistry that is concerned with electron transfer at the solution/electrode interface, where the electrode is an electrical conductor/semiconductor in an electrochemical cell. These observed processes are oxidation-reduction reactions. Chemical effects that occur during these reactions may be monitored by the current, potential or charge. As previously mentioned, surfaces roughened by electrochemical approaches are commonly used as SERS active substrates, and a number of electrochemical strategies have been developed for fabricating nanostructured electrodes for use as SERS substrates, including roughening by triangular-wave electrochemical ORCs, anodic potential step, and square-wave potential-pulses [46, 47]. These methods are categorized as dynamic electrochemical techniques, because

current is allowed to flow through the analyte solution. Amperometry and voltammetry are branches of dynamic techniques. In amperometry, a constant potential is applied to the working electrode, and current is measured as a function of time. In voltammetry, a time-dependent potential is applied, and the resulting current is measured as a function of that potential.

Both of these methods make use of an electrochemical cell consisting of three electrodes and a supporting electrolyte. A reference electrode (RE) maintains a constant potential under changing experimental conditions. The most commonly used REs are Ag/AgCl and Hg/Hg_2Cl_2 (standard calomel electrode, SCE) [48]. The working electrode (WE) is where the redox processes, or reactions of interest, occur. The potential of the WE, which is controlled by a potentiostat, is referenced against the RE potential. A counter electrode (CE) helps pass the current flowing through the electrochemical cell. The current, a measure of the rate of analyte oxidation or reduction, travels between the WE and the CE. The current and a potential cannot be simultaneously controlled.

The electrolyte is an ionic substance that is present in a solution to ensure conductivity. The electrolyte is typically an aqueous salt found at a concentration of 0.01-0.1 M, that does not undergo significant redox chemistry. The presence of oxygen in an electrolyte solution may interfere with interfacial electrochemical processes [48]. By purging the solution with an inert gas such as argon or nitrogen, these interferences can be eliminated. When preparing SERS active substrates by ORCs, a chloride electrolyte is often selected because it facilitates the metal dissolution–deposition process that is known to produce roughened surfaces [47].

2.7 Electron Microscopy

Electron microscopy (EM) is an analytical technique that was developed by Max Knoll and Ernst Ruska in the early 1930s, and involves the usage of an electron beam to form an image of a specimen [49]. The first transmission electron microscope (TEM) was designed in an effort to achieve a higher resolution than the optical microscope [49]. Unlike light microscopy, which uses a light source to illuminate a sample, and optical lenses for magnification, EM imaging occurs in a vacuum, and uses an electron beam as a source of illumination. Electromagnetic lenses magnify the image [50]. The resolution in microscopy is limited to about half of the wavelength of the illumination source. Electrons have a much smaller wavelength than visible light (e.g. λ = 0.005 nm at an accelerating voltage of 50 kV), which therefore allows for a much higher resolution than could be obtained with light [50]. By increasing the velocity of the electrons, and obtaining a shorter wavelength, an increase in resolving power occurs [50].

In TEM imaging, an electron beam is transmitted through a sample, typically a nano-material or biological structure, prepared across a thin support film. If a bulk material is being examined, it must be thinned down to the required nanometer-scale thickness [51]. All samples must be free of water, because the microscope vacuum prevents the direct observation of hydrated samples. Resolution is related mainly to beam coherence and brightness, as the stability of the high voltage and objective lens quality are well controlled [52]. In TEM, specimens can be magnified from 500 to 500,000 times, to produce a two-dimensional image [50]. The smallest analyzable size is from 2 to 1 nm [52]. This technique has proved useful for evaluating the size and shape of various

nanoparticles, and is the most used microscope technique for characterizing crystal defects at the atomic scale [53].

Scanning electron microscopy (SEM) is a commonly used technique for the observation of the morphology and composition of samples [53]. SE microscopes are equipped with a narrow incident electron beam that scans the sample in a convergent fashion, by sequentially moving the electronic probe. This displacement is achieved by using deflection coils [52]. The first published SEM images were by Knoll, in 1935 [49]. Unlike in TEM, SEM provides a three-dimensional image of a sample, but can only magnify the specimen from between 10 and 100,000 times [50], meaning the smallest analyzable size is 50 to 0.025 μm [52].

2.8 Energy Dispersive X-ray Analysis

Energy-dispersive X-ray spectroscopy (EDX) is an analytical technique used for elemental analysis. Typically, SEM and TEM instruments are equipped with EDX. This technique enables characterization of sample elemental composition by using X-ray emissions resulting from the bombardment of an electron beam on the sample [54]. The beam can interact with inner shell electrons in the atoms and knock them out of their orbital shell. Electrons in the outer orbitals with higher energy relax into these vacancies in the inner shell. During this process, the atom can release characteristic X-rays [54, 55]. Because the X-ray energy depends on the atomic orbital configuration of the target atoms, it can be used as a fingerprinting tool to identify the composition of the target [54]. Accordingly, EDX systems measure the energy of the X-rays that are generated and produce a spectrum that relates intensity (number of X-ray counts) to energy [55].

2.9 Ultraviolet-visible Spectroscopy

UV-vis spectroscopy is a widely used analytical technique for the quantitative or qualitative characterization of various materials. A sample is irradiated with electromagnetic waves in the UV and visible ranges of 200-800 nm, and the absorbance of the analyte over this region is monitored. There exist two typical UV-vis absorption set-ups: the single beam and double beam. In a single beam configuration, the spectrum of a reference in the cuvette is collected and stored, and then compared with the spectrum of the sample. In a double beam configuration, monochromatic light is split into two beams. One of them is passed through the sample, and the other passes through the reference. The two beams are then directed to detectors, and the output signals are compared to obtain a measurement [56].

UV-vis analysis is commonly used for the characterization of nanoparticles because it can provide information concerning size-dependent properties, through peak broadening and shifts in the absorption profile. Normally an absorbance maximum is observed in the spectrum (the λ_{max}), which corresponds to the LSPR of the nanoparticles. When the free electrons in the metallic structure are driven by the incident electric field to collectively oscillate at a certain resonant frequency, the incident light is absorbed by the particles [26]. Generally, AgNPs have a λ_{max} of approximately 400 nm, whereas the λ_{max} of gold nanostructures occurs at a higher wavelength [57]. There has been increased interest in research to control the tenability of plasmon resonances of nanoparticles over a broad spectral range, as it opens up opportunities in photonics, optoelectronic, biomedical, and spectroscopic fields [26]. For near-spherical particles, the greater the particle size, the longer the wavelength of the plasmon [57]. Varying the geometries to

produce nanorods, nanoprisms, nanoshells, nanostars, and nanocages, for example, also allows for a degree of control over the plasmon resonance. It can be noted that the efficiency of absorption and scattering for silver and gold is wavelength dependent.

Chapter 3: Experimental

3.1 General

Electrochemical and wet chemical methods (nanoparticle synthesis) were used to roughen the metal coating on silk fibers and fabric chips. The prepared nanoparticles were characterized by UV-vis spectroscopy, SEM, and TEM imaging. All roughening methods were evaluated by SEM imaging, and by the SERS signal of 4,4'-bipyridine (4,4'-byp) on the modified fabric substrates. The methods that displayed the most promising results were chosen as SERS substrates for the detection of biomolecules 2'-deoxyguanosine 5'-monophosphate (dGMP), guanosine, and guanine. These substrates were selected based on a strong 4,4'-byp SERS signal and a relatively large signal-to-noise ratio in the corresponding SERS spectra.

3.2 Reagents

4,4'-Byp, dGMP (≥ 98 %), guanosine (≥ 98 %), guanine (98 %), sodium citrate (≥ 99 %), L-ascorbic acid (≥ 99 %), poly(diallyldimethylammonium chloride) (PDDA) solution (35 wt%), hydroxylamine hydrochloride ($NH_2OH \bullet HCl$, 99.999 %), and gold(III) chloride hydrate ($HAuCl_4 \bullet xH_2O$, ≥ 99.9 %) were purchased from Sigma Aldrich (St.Louis, MO). Silver nitrate (99.9995%) was purchased from Alfa Aesar (Wardhill, MA), potassium biphthalate was purchased from ACP Chemicals Inc. (Montreal, QC), potassium chloride was purchased from Fisher Scientific (Fair Lawn, NJ) and sodium borohydride ($NaBH_4$, 99 %) was purchased from Fluka Analytical (Seelze, Germany). All chemicals were used without further purification. All solutions were prepared using Millipore water (solution resistivity >18.2 MΩ•cm). Sodium

hydroxide (NaOH, 1.0 M) was added to guanosine and guanine solutions, to ensure dissolution (pH = 11). Glassware was cleaned in a sulphuric acid bath and thoroughly rinsed with Millipore water (solution resistivity >18.2 MΩ•cm). Achira Labs, in Bangalore, India, supplied fibers and fabric samples.

3.3 Characterization of Samples

Imaging of the fiber and fabric samples was performed using a LEO 1450 VP SEM (Saint Mary's University, Halifax, N.S.), having a maximum resolution of up to 3.5 nm at 30 kV, equipped with an INCA X-max 80 mm^2 EDX system that used Silicon Drift Detector technology to analyze characteristic X-rays emitted from the sample. Various spots on a single sample were selected for EDX analysis, based on the SEM images, to collect semi-quantitative elemental information. A Hitachi S-4700 FEG SEM (Dalhousie University, Halifax, N.S.), which had a maximum resolution of 1.5 nm at 1.5 kV, was also used to image the treated fabric samples. Characterization of nanoparticles was carried out by means of a TEM (FEI, Tecnai 12; operating at an acceleration voltage of 120 kv), at Dalhousie University, Halifax, N.S. Colloid samples were deposited on copper grids (Sigma Aldrich, St. Louis, MO) prior to centrifugation or washing, with the exception of the truncated octahedral gold nanoparticles (TOC AuNPs), which were washed before deposition. Size distributions of the colloids were calculated from ImageJ 1.47, a public domain image-processing program (National Institutes of Health, USA). Absorption data for the colloidal solutions was collected using a Cary 100 UV-Vis spectrophotometer (Agilent Technologies, Mississauga, ON, Canada).

3.4 Raman Spectrometer Setup

Raman and SERS measurements were initially recorded using a previously described portable SERS set-up [58]. However, the vast majority of all experiments were conducted using a Thermo Scientific DXR SmartRaman spectrometer (Thermo Fisher Scientific, Mississauga, ON, Canada) equipped with an air-cooled CCD detector, 780 and 532 nm diode lasers, as well as a laser line filter. The maximum power output of the 532 nm and 780 nm lasers was 10 mW and 150 mW, respectively. A high-resolution grating was used to collect the Raman signal within the range of 200 to 1800 cm^{-1}. All SERS spectra were collected at laser powers between 2.0-70.0 mW and for acquisition times of 20-60 seconds. The spectrometer resolution was 3 cm^{-1}. Fabric samples were mounted using a support, which compressed the sample, holding it perpendicular to the laser beam. A minimum of 5 SERS spectra were collected at various spots on each fabric sample treated with nanoparticles. A single spectrum was collected for all normal Raman spectra. Data processing involved correction for power and time, and smoothing by adjacent averaging of 8 points, using Origin 8.1 software (OriginLab Corporation, Northhampton, MA, USA).

3.5 Removal of Copper Oxides from Fiber Samples

For SERS analysis, it is desirable that the metal substrate be free of any contaminants which could block the analyte from adsorbing onto its surface. It is reported that organic acids can complex with copper ions, removing any metallic ions or metallic contaminants from the substrate [59]. Citric acid, in particular, is known to be a complexing agent for copper ions and is used in many cleaning processes [59]. Rather than mechanically removing any surface contaminants through the use of alumina

powder, which is commonly employed for polishing electrodes, citric acid was used. This method, unlike polishing, prevented the underlying silk fibers from being damaged. The metal-coated fiber samples were therefore incubated in solutions of 5% citric acid and 10% citric acid for 3 or 24 hours, and analyzed by SEM imaging.

3.6 Electrochemical Roughening of Metal-Coated Fibers

Silk fibers were roughened using a Princeton Applied Research 273A potentiostat/ galvanostat, in a three-electrode setup. A platinum CE and a Ag/AgCl RE were used. The metal-coated fiber served as the WE. Similar to procedures developed by Kudelski *et al*. [60], the metal coating was subjected to the following roughening procedures: (i) 25, 29, or 50 successive positive scans at 500 mV/s from 0.4 to -0.4 V, or 1.0 to 0.4 V in KCl (0.1 M); (ii) 25 successive positive-negative scans at 500 mV/s from 1.0 to -0.4 V in either, KCl (0.1 M), H_2SO_4 (0.1 M), or a solution containing $CuSO_4$ (0.2 M) and H_2SO_4 (0.1 M); (iii) Anodic dissolution in either KCl (0.1 M), H_2SO_4 (0.1 M), or a solution containing $CuSO_4$ (0.2 M) and H_2SO_4 (0.1 M) at 0.425 V for 30 s. For SERS measurements, samples were incubated in a 1.0 mM 4,4'-byp solution for 30 minutes, then removed and air-dried. The fiber was then knotted to increase the diameter of the fiber, for easier spectral collection.

3.7 Modification of Fabric Chip using Nanoparticles

Fabric samples (3.0-6.0 mg, approximately 5-8 mm^2) were treated with various nanoparticles, as described below. For SERS measurements, 40 μL of 1.0 mM 4,4'-byp solution were deposited on the samples and allowed to air-dry, with the exception of the silver microspheres.

3.7.1 Citrate-Reduced Silver Colloids

Citrate-reduced silver colloids were prepared according to a modified Lee and Meisel reduction [61]. Briefly, an aqueous sodium citrate solution (25 mL, 0.1 wt %) was added to a boiling $AgNO_3$ solution (50 mL, 0.10 mM), and boiled for 30 minutes. Once cooled to room temperature, fabric samples were incubated in the formed colloidal suspension for 1 hour and allowed to air-dry. To form a AgNP "paste", 1.0 mL aliquots of the colloidal suspension were added to Eppendorf tubes and centrifuged at 3600 rpm for 15 minutes. The supernatant was removed and discarded, and another 1.0 mL aliquot of the suspension was added to the tube. This process was repeated ten times. 20 μL of the concentrated AgNPs were deposited on a fabric chip, and allowed to dry. This paste was also deposited on a glassy carbon screen-printed electrode (3 layers of 5 μL). Another experiment was conducted, during which the fabric chip was added to the $AgNO_3$ solution before the reducing agents. After this *in situ* synthesis, the fabric chip was removed from the solution and dried.

3.7.2 Modified Citrate-Reduced Silver Nanoparticles

Following a method described by Zhao [62], to 95 mL of water in a three-necked round bottom flask, solutions of $AgNO_3$ (1.00 mL, 0.1 M), sodium citrate (3.40 mL, 0.17 M) and citric acid (0.600 mL, 0.17 M) were added and stirred under reflux. $NaBH_4$ (0.200 mL, 0.1 mM) was added to this mixture, which was then heated to a vigorous boil. The colloidal suspension was removed from the heat after 1 hour. Fabric samples were incubated in this solution for 1 hour, then removed and air-dried. An *in situ* method for modifying the fabric using these nanoparticles was attempted, in which the fabric sample

was added to the initial silver solution, before the addition of $NaBH_4$. At the end of the synthesis, the fabric was removed and allowed to dry. A second *in situ* method was explored, in which the fabric sample was added to the solution at the same time as the $NaBH_4$.

3.7.3 Silver Microspheres with Nanofeatures

Silver microspheres possessing uniform nanofeatures were prepared as reported by Huang and Zhu [63]. Briefly, a potassium biphthalate solution (20 mL, 12.5 mM) was added to a solution of $AgNO_3$ (1.0 mmol in 10 mL). L-ascorbic acid (10 mL, 0.1 M) was then added to the mixture under constant stirring. After 2 hours, a precipitate was formed, washed (in ethanol, followed by water), isolated and dried. The resulting precipitate was imaged by SEM, directly on carbon tape. Solutions of 10 mM, 50 mM, 100 mM, and 200 mM silver microspheres, were prepared in 4,4'-byp (1.0 mM) and allowed to sit for 24 hours. These solutions were stirred prior to deposition (40 μL) on fabric samples, which were then air-dried. SEM images of these surfaces were collected. In another experiment, fabric samples were incubated in solutions of 100 mM and 200 mM microspheres. An *in situ* method was also performed, during which a fabric sample was added to the initial $AgNO_3$ solution, and removed after the synthesis.

3.7.4 Gold Nanoparticles

AuNPs were prepared according to the synthesis described by Ji *et al*. [64] Aqueous $HAuCl_4$ (0.25 mM) was prepared, then brought to a boil, with stirring. Aqueous sodium citrate (5%) was added to this solution. The reaction was allowed to run until the solution reached a ruby red color, indicating completion. Fabric samples were incubated

in the colloidal suspension for 1 hour, then removed and air-dried.

3.7.5 Gold Nanostars

The preparation of seed-mediated nanostars was carried out following a synthesis reported by Yuan *et al*. [65]. Gold seeds were first prepared by adding a sodium citrate solution (15 mL, 1 wt/vol %) to an aqueous $HAuCl_4$ solution (100 mL, 1.0 mM). This seed solution was then filtered through polyvinylidene difluoride (PVDF) 0.2 μm syringe filters. The seed solution was added to a solution of $HAuCl_4$ (10 mL, 0.25 mM) with HCl (10 μL, 1 M) followed by the simultaneous addition of L-ascorbic acid (100 μL, 0.1 M) and $AgNO_3$ (100 μL, 3 mM) solutions. This resulted in the formation of a blue-green solution, which was centrifuged for 25 minutes at 1500 rpm and redispersed in ~7 ml of water. Fabric samples were incubated in the final solution for 1 hour, then removed and air-dried.

3.7.6 Gold Nanoflowers

Gold nanoflowers (AuNFs) were prepared following a synthesis described by Zhao *et al*. [66] Briefly, a $HAuCl_4$ solution (3.775 mL, 0.27 mM) was prepared, to which a solution of NaOH (6 μL, 1 M) was added to adjust the pH. A gold seed solution (600 μL) was combined with $NH_2OH \bullet HCl$ (60 μL, 44.4 mM, pH 11). The resulting seed solution (330 μL) was added to the gold solution. To prevent aggregation, the colloidal solution was centrifuged at 1500 rpm for 5 minutes, and re-suspended in water. Fabric samples were incubated in this solution for 1 hour, then allowed to air-dry.

3.7.7 Truncated octahedral (TOC) nanoparticles

TOC AuNPs were synthesized as reported by Li and Ma [67]. The synthesis involved adding solutions of PDDA (800 μL, 100 mg mL^{-1}) and $HAuCl_4$ (320 μL, 4.5 mM) to a round bottom flask containing 40 mL of water. The solution was then heated under reflux for 1 hour, until a color change from colorless to pink was observed. The colloidal solution was a very pale pink color, suggesting it was very dilute. 1.00 mL aliquots of the solution were centrifuged for 15 minutes at 1000 rpm, then the supernatant was removed and another aliquot was added to the Eppendorf tube. This was repeated 8 times. The final concentrated nanoparticles were redispersed in 2 mL of water. A fabric sample was incubated in these nanoparticles for 1 hour, and then air-dried.

Chapter 4: Results and Discussion

4.1 Characterization of Fabric Chip

Achira Labs, in India, prepared the fabric samples used in this work. This lab manufactures various metal-coated silk fibers and fabrics on a large scale. These silk fibers were characterized using SEM, EDX and Raman spectroscopy. The SEM images in Figure 3 show that the metal coating on the silk was wrapped in such a way that gaps exposed a small area of the silk. It may also be noted that the metal was very smooth.

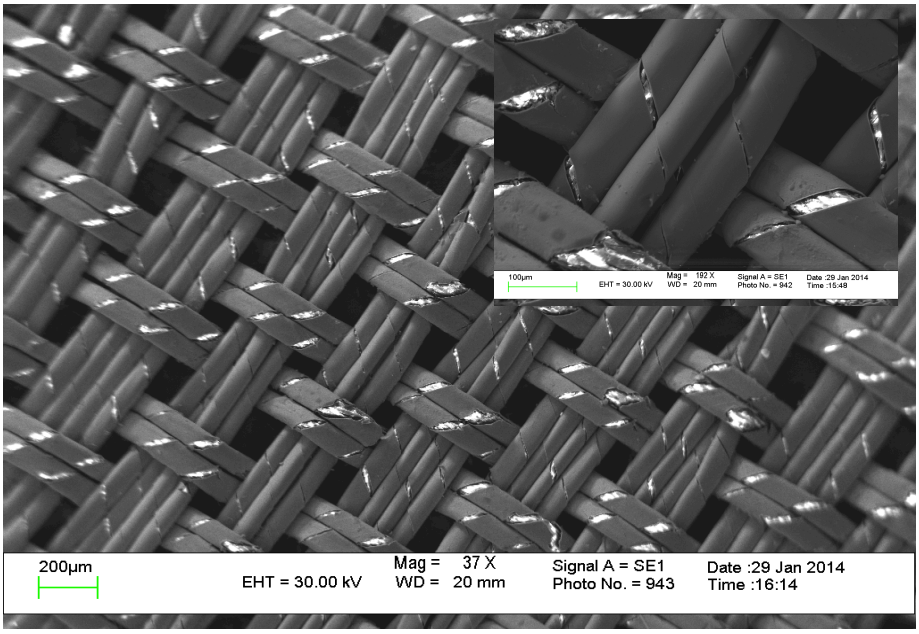

Figure 3. SEM image of metal-coated fabric sample, produced by Achira Labs. Inset shows a higher resolution image of the fabric.

The composition of the metal on the silk was determined using EDX analysis, which provided the elemental composition of the metal surface. It was found that carbon (40.04%), nitrogen (7.72%), oxygen (8.55%), aluminum (0.08%), copper (32.65%), zinc (9.68%), and silver (1.17%) were the main constituents of the fabric. It appears the metal could be brass. The percentages of these elements were determined by averaging the

EDX data collected on 7 different spots. The carbon, nitrogen, and most likely a portion of the oxygen, resulted from the underlying silk. It can therefore be said that copper was the main constituent of the metal. Phosphorus, sulphur, chloride and chromium were also present on some spots, in trace amounts. These elements are suspected to be contaminants on the surface.

4.2 Normal Raman 4,4'-Bipyridine (4,4'-byp)

In order to evaluate the various roughening procedures undertaken in this work, the Raman signal of 4,4'-byp was used. 4,4'-Byp displays a strong Raman signal, and numerous SERS studies using this molecule to investigate SERS substrates have been performed [68]. The strong signal is due to the extensive π-bond conjugated system of the pyridyl rings and the presence of two active nitrogen atoms, which enables electron transport, as well as energy transfer processes [69]. Both the normal Raman and SERS signal of this molecule were collected and are shown in Figure 4. The SERS spectrum was collected on a AgNP-coated glassy carbon screen-printed electrode, a reliable SERS-active substrate [58], which provided an idea of band shifts that may occur during SERS measurements relative to the normal Raman signal.

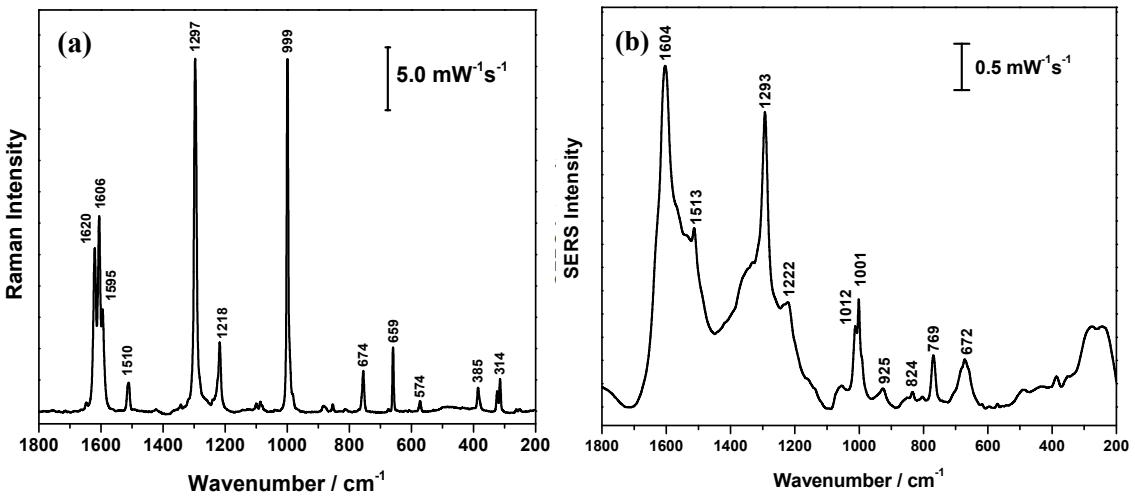

Figure 4. (a) Normal Raman signal of pure 4,4'-byp powder (532 nm, 10 mW, 30 s) and (b) SERS of 4,4'-byp (0.1 M) solution drop coated on a AgNP-coated glassy carbon screen-printed electrode (average of 10 spectra, 532 nm, 5 mW, 60 s).

The band assignment for the normal Raman and SERS signals of 4,4'-byp is displayed in Table A-1. The most intense bands, at 1603, 1293 and 1001 cm^{-1} in the SERS spectrum, corresponding to C-C ring stretching, inter-ring stretching and ring breathing modes, respectively, were chosen to be the marker bands for this compound, when detected on the fabric samples. It is important to note that the background was significant in the SERS spectrum of 4,4'-byp (Figure 4 *b*). This is most likely due to the incomplete formation of a film on the surface of the electrode, because rather than performing an incubation, the 4,4'-byp was deposited on its surface. This was done to best mimic the way by which 4,4'-byp would be detected on the fabric samples, as the model constructed herein uses the fabric chip as a substrate for the rapid detection of a fluid with which it came into contact, rather than a fluid in which it was incubated**.**

4.3 4,4'-Bipyridine on Untreated Fabric

Collection of the SERS signal for 4,4'-byp was attempted on the fabric surface, prior to any roughening treatment. As expected, the signal was weak and very noisy, due to the lack of nanofeatures, which give rise to the SERS effect. No peaks corresponding to the Raman signal of 4,4'-byp were observed. Nonetheless, this study was valuable, as it demonstrated that the gaps between the metal coating expose the silk fibers, which give rise to a Raman signal for silk. Silk is a fibrous protein, which consists mainly of glycine, alanine and serine [70]. It was possible that the Raman signal of silk could interfere with the analyte signal. For this reason, the normal Raman of the fabric sample was recorded, using both the 532 nm and 780 nm laser. These spectra are shown in Figure 5.

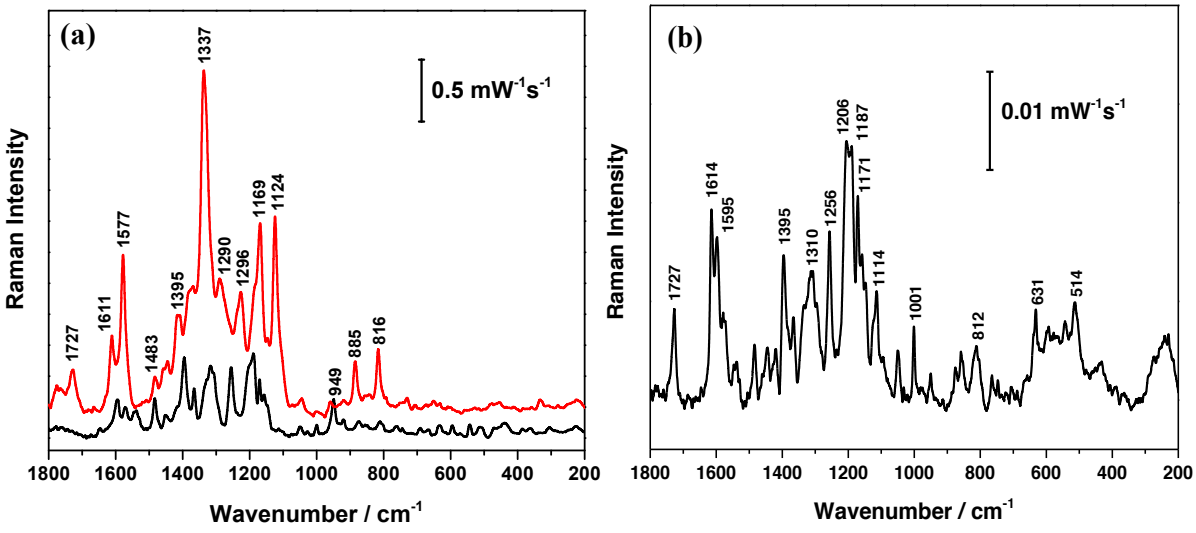

Figure 5. Normal Raman spectrum of silk, collected using a (a) 532 nm laser, at 10 mW for 40 seconds at two different spots and a (b) 780 nm laser, at 150 mW, for 60 seconds.

The Raman signals in Figures 5 *a* and *b* were quite weak and noisy; this is due to the fact that silk is a weak Raman scatterer, and normal Raman is less sensitive than SERS. It may also be noted that different bands with varying intensities appeared in the spectrum depending on the excitation source. Additionally, Figure 3 *a* shows that a different silk

signal could appear at different spots on the fabric. Nevertheless, the bands labelled in these spectra correspond well to those reported for silk, in the literature [70, 71]. A complete band assignment is provided in Table A-2.

For further detection of analytes, it was desirable to minimize or eliminate the silk Raman signal. This could be achieved by successfully roughening the metal coating on the silk, which would enhance the analyte SERS signal, or by coating the silk in a roughened metal. Both of these options were explored through electrochemical and wet chemical methods.

4.4 Removal of Copper Oxides from Fibers

It is suspected that copper oxides quench the SERS signal, making it difficult to detect a given analyte [52]. Work by Ko and Lee [72] demonstrated that copper oxides, specifically CuO and CuO_2, on the surface of an electroplated copper surface could be dissolved in an aqueous citric acid solution as confirmed by X-ray photoelectron spectroscopy (XPS). Additionally, it was shown by atomic force microscopy that treatment in citric acid also increased surface roughness. This method of treatment therefore appeared to be an ideal way of cleaning the metal surface of the fibers used in this work, which would be evidenced by increased roughness. However, the SEM images of the fiber samples treated in aqueous citric acid solution did not display any surface roughness. It appeared that no significant morphological changes had occurred on the metal during this treatment. This may have been due to the fact that the metal coating was an alloy, reducing the presence of copper oxide contaminants. It would have been advantageous to use XPS to examine these fibers rather than EDX, as it would provide accurate data on the type of oxides present and their respective quantities on the metal

substrate. This instrument was however unavailable, and many alternatives for reliably modifying the metal substrates were available. Electrochemical roughening and nanoparticle treatment were therefore pursued.

4.5 Electrochemical Roughening of Fibers

Electrochemical roughening procedures were carried out in three different solutions. This method of roughening the metal coating of the silk proved to be difficult, because the fibers would often drift in solution and come into contact with either the RE or CE. This said, in most cases, roughening did occur on the fiber samples during ORCs. The anodic dissolution procedure, during which the potential of the fiber was held constant for 45 seconds in an electrolyte solution, did not roughen the metal coating.

Before and after SEM images in Figure 6 show that the electrochemical roughening procedures in a solution of $CuSO_4$ and H_2SO_4, as well as a solution of KCl were successful, although the roughening was not uniform.

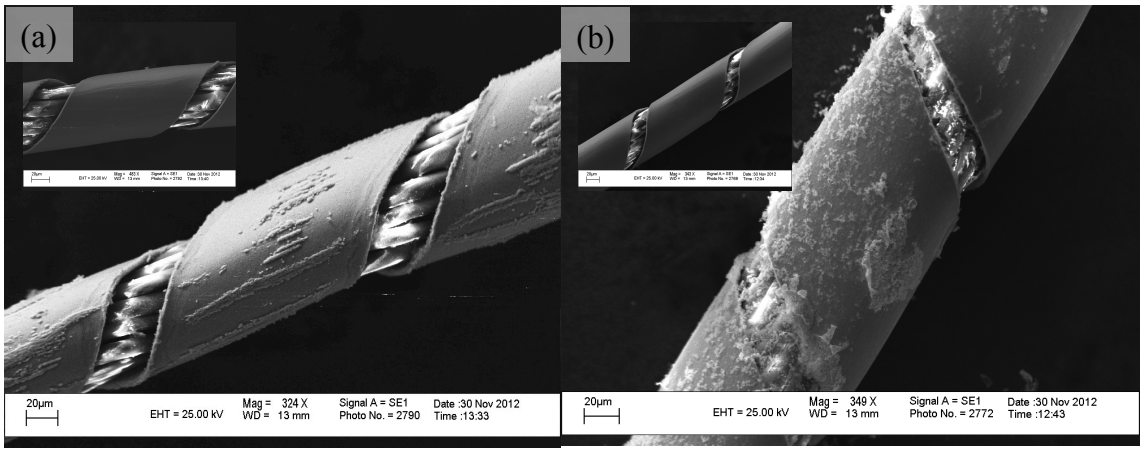

Figure 6. SEM image of a metal-coated fiber electrochemically roughened by ORC treatment in (a) $CuSO_4$ (0.2 M), H_2SO_4 (0.1 M) solution and (b) ORC treatment in KCl (0.1 M).

It may be noted that chloride salts are the most commonly used electrolytes for ORC treatments, because they assist in the metal dissolution-deposition process that is known to produce SERS-active roughened substrates [73]. In fact, the fiber sample subjected to 25 successive positive scans at 500 mV/s from 1.0 to -0.4 V in KCl (Figure 6 *b*) showed the greatest extent of roughening, although the fiber treated in the $CuSO_4$ •H_2SO_4 solution (Figure 6 *a*), using the same electrochemical parameters, displayed a slightly more uniform roughening pattern. EDX data was collected, to gain a better understanding of what had occurred at the metal surface. It was found that the roughened portion of the metal on the samples shown in Figure 6 *b* consisted of copper (18%), silver (57%), gold (5%), chloride (11%) and oxygen (9%). It is suspected that chloride and oxide species were present on the substrate, which is consistent with the literature [52].

To verify the SERS-activity of the roughened fibers, SERS spectra of 4,4'-byp were collected using a portable SERS setup. The portable Raman system was used because it enabled the manual focusing of the laser on the samples. This was important because the fibers were knotted, to ensure that their diameter was as large as the laser beam. The spectra collected on the sample roughened by ORC treatment in KCl are displayed in Figure 7.

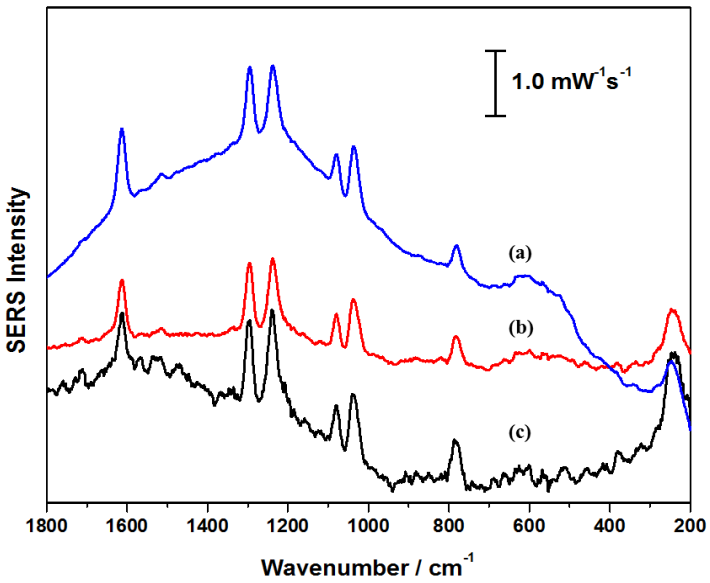

Figure 7. SERS signal of 1.0 mM 4,4'-bipyridine on fiber sample at different powers; (a) 22.3 mW, (b) 10.6 mW, and (c) 2.93 mW, using a 785 nm bench top spectrometer.

These spectra show well resolved peaks at 1600, 1294, 1218, 1020, and 770 cm^{-1}, all of which correspond to 4,4'-byp. At higher powers, the background in the spectra became more pronounced (Figure 7 *a*), which could be a result of light shining through the knot, or that part of the knot was raised, and not at the focus distance of the laser. It is also possible that photodegredation of the sample took place, also contributing to the background in the spectra. Spectra collected on the other electrochemically-roughened fibers were either plagued by noise, making the detection of 4,4'-byp difficult, or no SERS signal of 4,4'-byp could be observed at all. It was suspected the enhancement provided by these SERS substrates would be insufficient for the detection of trace levels of analyte. For that reason, alternative methods for roughening the metal-coated silk were pursued.

4.6 Treatment of Fabric with Nanoparticles

Silver and gold nanostructures were prepared for the modification of the fabric samples. In the literature, treatment of fabrics with nanoparticles is typically undertaken to provide new properties, such as UV-blocking, water repellency, and antimicrobial properties [74]. The selected nanoparticle preparations were chosen based on their straightforward syntheses, which did not require the use of surfactants or stabilizing agents, with the exception of the TOC AuNPs. Surfactants and stabilizing agents are undesirable for the design of nanoparticles for SERS, despite their ability to control the size and shape of nanoparticles. Surfactants may contribute to large background signals during the detection of an analyte by SERS due to their strong surface adsorption [75].

4.6.1 Characterization of Nanoparticles

4.6.1.1 Citrate-Reduced Silver Colloids

AgNPs were prepared by a standard citrate reduction and characterized by TEM imaging and UV-vis spectroscopy, as shown in Figure 8.

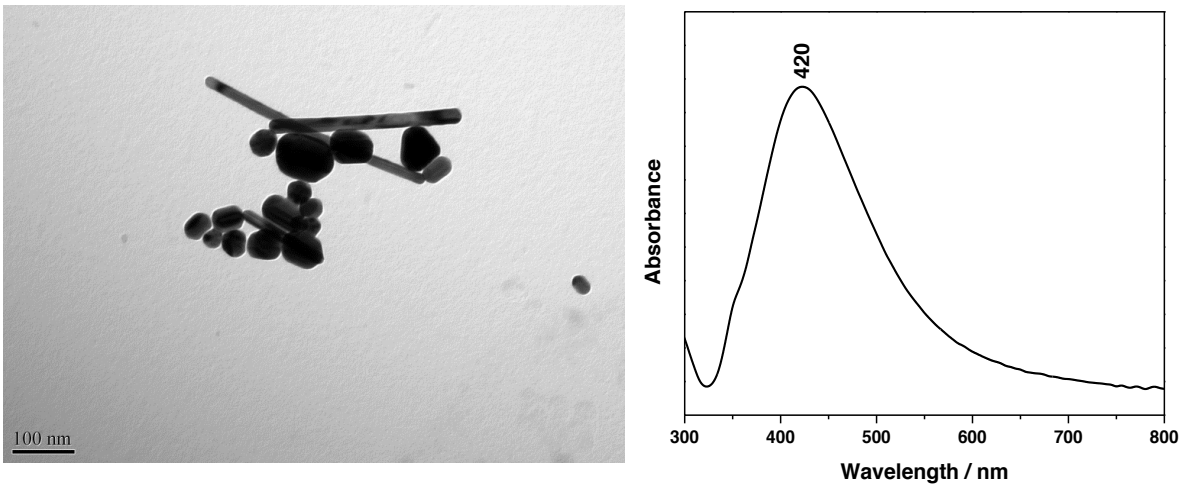

Figure 8. TEM image of citrate-reduced AgNPs (105, 000 x), and the corresponding UV-vis spectrum of the colloids.

The TEM image revealed that these nanoparticles were quite irregularly shaped and had a wide size distribution. The average diameter of the AgNPs was found to be 50 ± 19 nm, assuming the nanoparticles were spherical. This value, therefore does not account for the rods present in solution, which measure up to several hundreds of nm. It is evident that this synthesis did not allow precise control over the nanoparticle growth. The broad absorbance band in the UV-vis spectrum provided further indication of the large size distribution of the colloids. Nonetheless, the λ_{max} of these colloids was 420 nm, which is consistent with previously reported data [69].

4.6.1.2 Modified Citrate-Reduced Silver Nanoparticles

A TEM image and the UV-vis absorbance spectrum of silver nanoparticles prepared by the reduction of $AgNO_3$ by $NaBH_4$ and sodium citrate are shown in Figure 9. From the TEM image, it was determined that the approximate size of these nanoparticles was 25 ± 6 nm. In comparison to the regular citrate-reduced AgNPs (Figure 8), these

nanoparticles were much more spherical and uniform, which is reflected by the narrow absorbance band in the UV-vis spectrum.

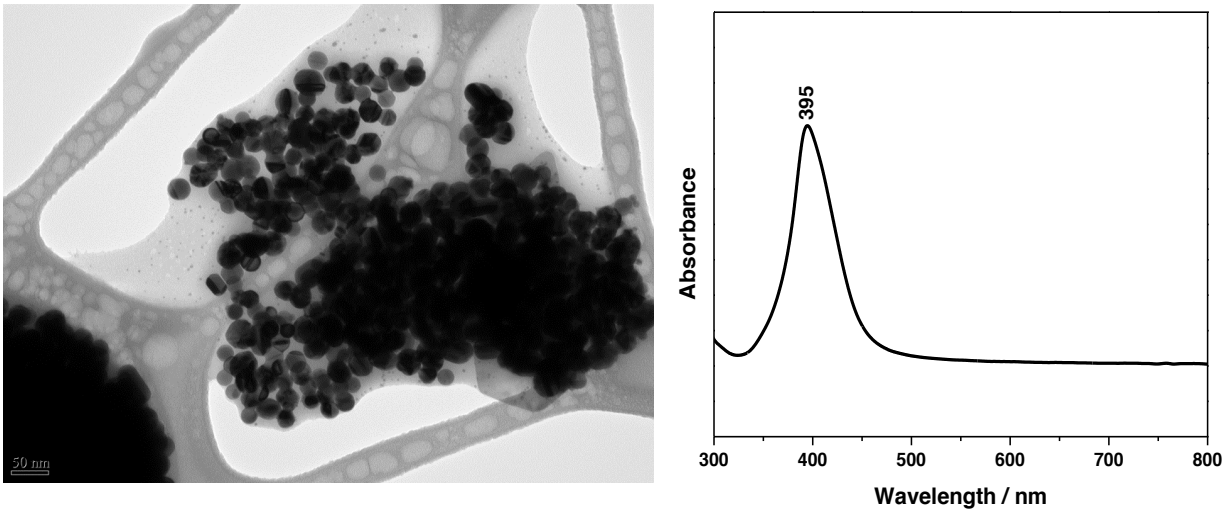

Figure 9. TEM image of the modified citrate-reduced Ag colloids (150, 000 x) by Lili Zhao, and UV-vis spectrum of the corresponding AgNPs.

The λ_{max} of these colloids occurred at 395 nm, deviating slightly from the reported literature value of 410 nm [62]. This discrepancy is negligible, because the nanoparticles were uniform and therefore provided a more reproducible SERS substrate than the regular citrate-reduced nanoparticles. It can be noted that aggregation of the nanoparticles was prevalent in solution. This could be advantageous, as partial aggregation of metal colloids generates greater SERS signals [58]. Concurrently, aggregated colloids can coagulate, rendering them unstable, which results in poor reproducibility of SERS [58]. For this reason, these nanoparticles were used for SERS measurements within a number of days, if not hours, of their synthesis.

4.6.1.3 Silver Microspheres with Nanofeatures

Silver microspheres covered in uniform nanofeatures were prepared. The handling of these structures was quite simple, because they crashed out of solution as a dark brown precipitate. Due to the nature and size of these particles, TEM was not used for their characterization, but rather SEM imaging. Six images of the silver microspheres are displayed in Figure 10.

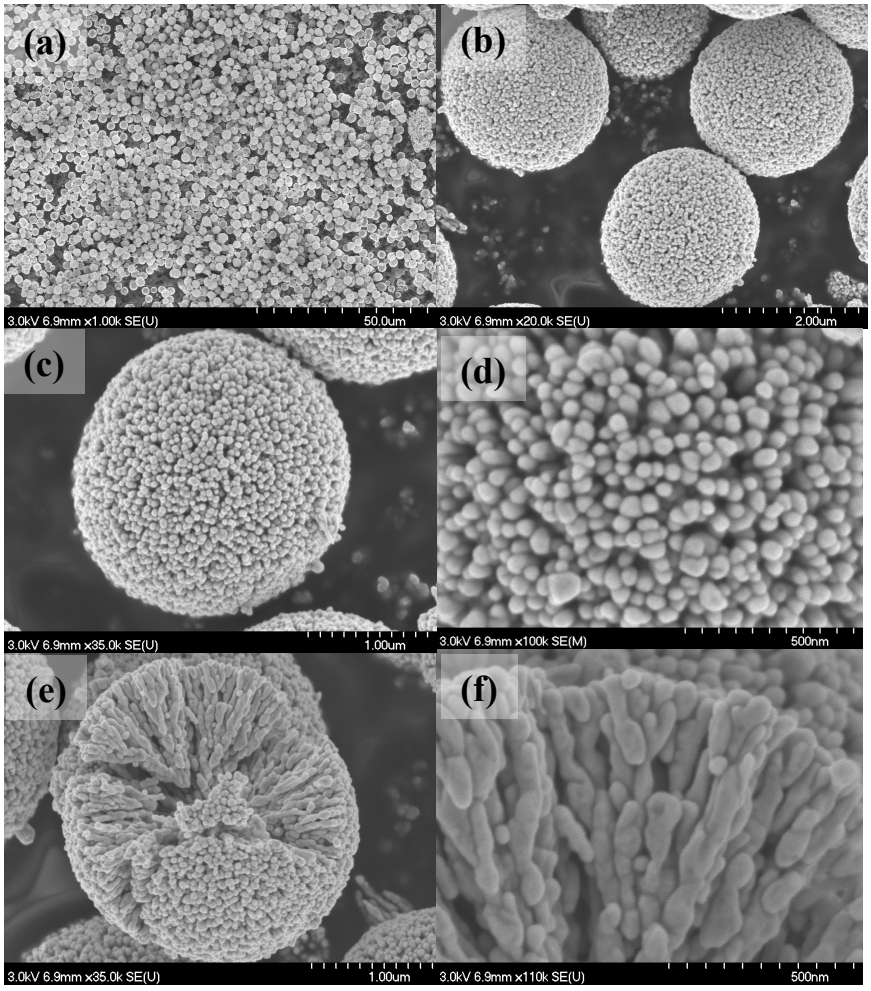

Figure 10. SEM images of (a, b) silver microspheres at low magnification, (c) single microsphere, (d) high magnification of nanofeatures on a microsphere and, (e, f) the broken microspheres.

The structure of the silver microspheres was indistinguishable from that reported by Huang and Zhu [63], which was promising because the SERS signal of rhodamine 6G at low concentrations (10^{-7} M) had been successfully collected on these silver structures.

The microspheres ranged from approximately 1.5-2.0 μm in size, and had nanofeatures of approximately 50 nm in diameter on their surface. The high magnification of a fragment of a broken sphere (Figure 10 *f*) revealed that the structures were built from radially oriented dendrites. This growth is thought to be a process of coordination—reduction—self-assembly, and the possible reactions occurring in solution are the following [63]:

$$2Ag^{+} + C_8H_4O_4^{2-} \rightarrow Ag_2C_8H_4O_4 \downarrow \text{(precursor)} \quad (1)$$

$$Ag_2C_8H_4O_4 + C_6H_8O_6 \rightarrow 2Ag\downarrow + C_6H_5O_6 \quad (2)$$

4.6.1.4 Gold Nanoparticles

AuNPs were prepared and characterized by Lili Zhao. As shown in the TEM image of these colloids, Figure 11, the average size of these NPs was approximately 23 ± 4 nm. This is consistent with previous studies of these nanoparticles [64]. The UV-vis spectrum of these nanoparticles is also provided in Figure 11, and shows that the λ_{max} for these colloids was 519 nm.

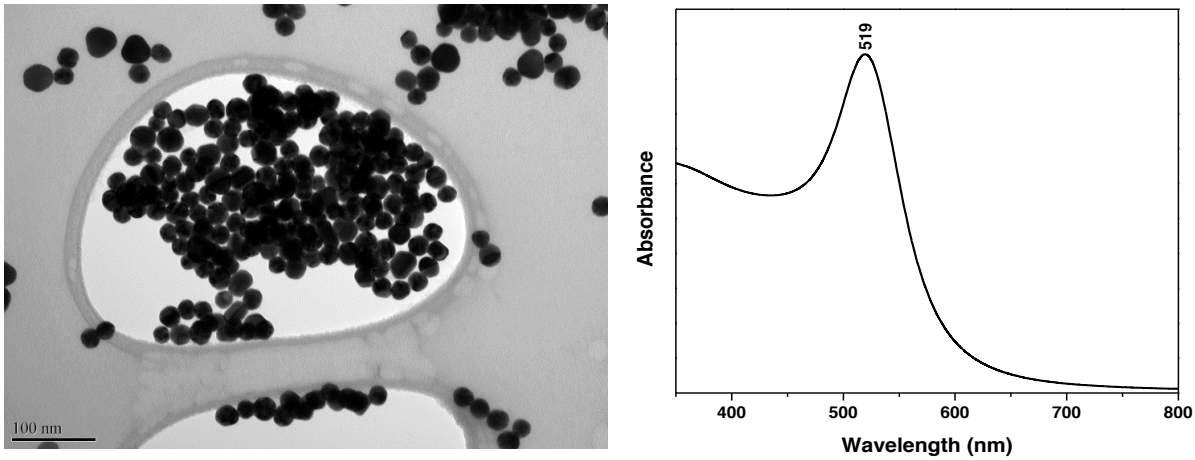

Figure 11. TEM image of citrate reduced AuNPs (180, 000 x) by Lili Zhao, and the corresponding UV-vis spectrum of the Au colloids.

4.6.1.5 Gold Nanostars

Gold nanostars were characterized by TEM and UV-vis spectroscopy, as shown in Figure 12.

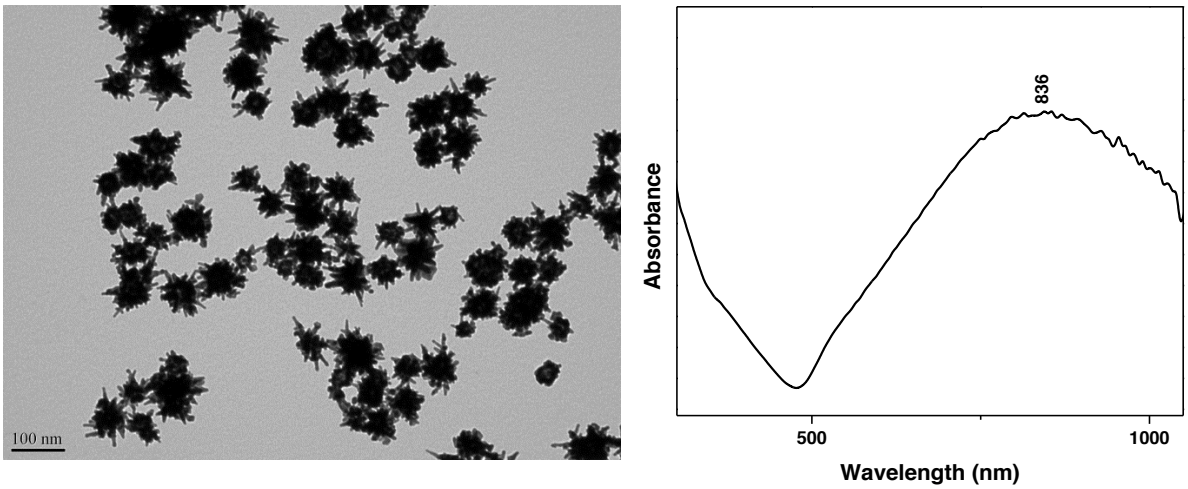

Figure 12. TEM image of gold nanostars (105, 000 x), and UV-vis spectrum of the corresponding sample.

The TEM image revealed that each nanoparticle possesses branch-like structures, giving them the characteristic star-like appearance. The average size of these nanoparticles was

56 ± 15 nm, which conforms to the reported value of 60 nm [70]. The UV-vis spectrum was broad, possibly due to the heterogeneous branch morphology, causing nanostar ensembles to enable a wider range of LSPR modes [65]. Despite the appearance of the nanostars being consistent with that reported by Yuan et al. [65], the UV-vis analyses of three separate, but identical, syntheses revealed significant inconsistencies in the absorbance of these colloids. The overlay of the collected spectra is shown in Figure 13, revealing that the λ_{max} ranged from ~660 to 870 nm.

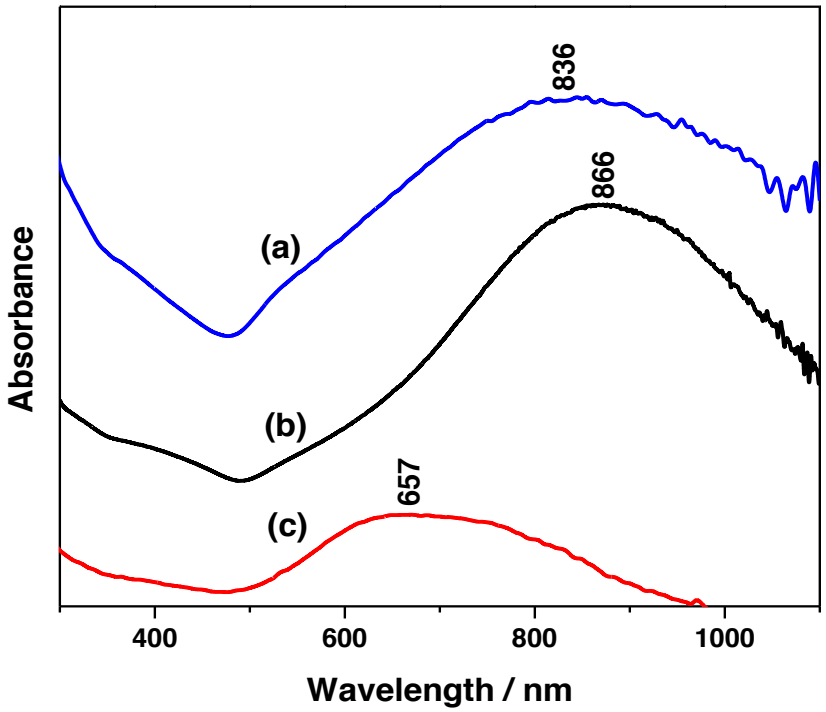

Figure 13. UV-vis spectra of gold nanostars synthesized on three different occasions, following the same protocol.

This result is possibly due to small variations that occurred during the mixing of the reagents. More specifically, the simultaneous addition of the ascorbic acid and silver nitrite solutions appeared to be the most critical step, as a color change was observed immediately after, and the reaction was completed within seconds. If the two solutions

were added at different rates, the resulting colloidal solutions would have different absorbance spectra. Yuan *et al.* [70] noted that the ascorbic acid must be added quickly and in a drop-wise fashion, to lead to sphere formation and that it must be added at the same time as silver. If the silver is added too late, larger gold spheres will be present in solution and the growth of the stars will not proceed as expected.

4.6.1.6 Gold Nanoflowers

A rapid and simple synthesis for gold nanoflowers was carried out. TEM and UV-vis spectroscopy were used to characterize the formed colloids, as shown in Figure 14.

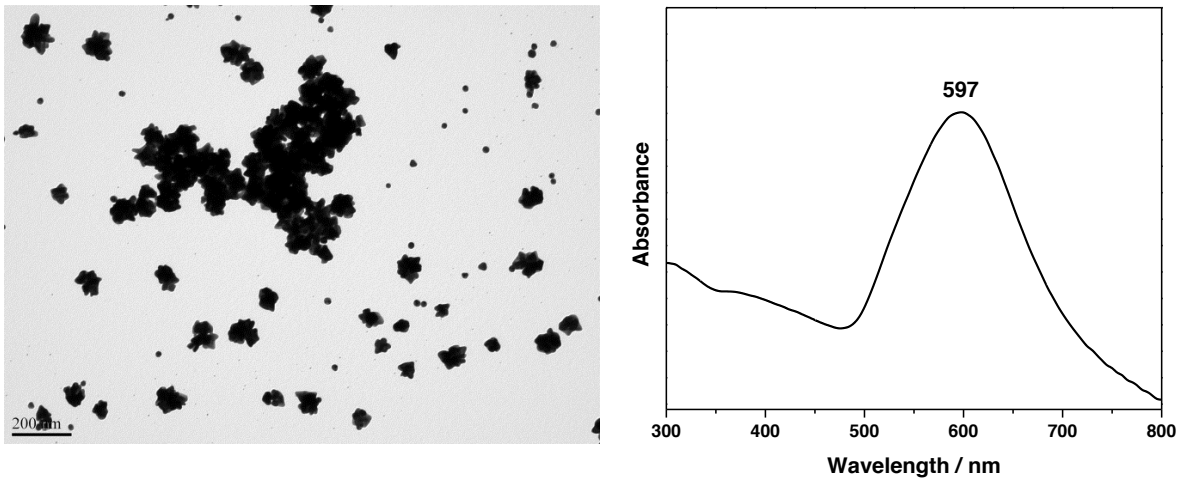

Figure 14. TEM image of AuNFs (60,000 x), and corresponding UV-vis spectrum of the colloids.

The gold nanoflowers were not centrifuged prior to collecting the TEM, therefore small particles (< 50 nm in size), which would be removed during centrifugation, are included in the image. The size of the nanoflowers, excluding the small particles, was found to be 82 ± 18 nm. This value is slightly greater than the reported value of 53 nm (± 15%) reported by Zhao *et al.* [66] The λ_{max} in the UV-vis spectrum was consistent with the literature. It can be noted that if the pH of the solution was not adjusted by NH_2OH, the

shape of the nanoflowers was altered, and the absorbance was blue-shifted.

4.6.1.7 Truncated Octahedral Gold Nanoparticles

The synthesis of TOC AuNPs utilized PDDA, a nontoxic and water-soluble cationic polyelectrolyte (Figure A-1), as both a reducing and stabilizing agent. The TEM image and UV-vis spectrum of the TOC NPs are shown in Figure 15. It is important to note that the colloids were centrifuged and redispersed in a small amount of water to increase their concentration, as the original solution was too dilute to obtain a UV-vis spectrum. Only a minor color change from translucent to pink could be observed during this synthesis.

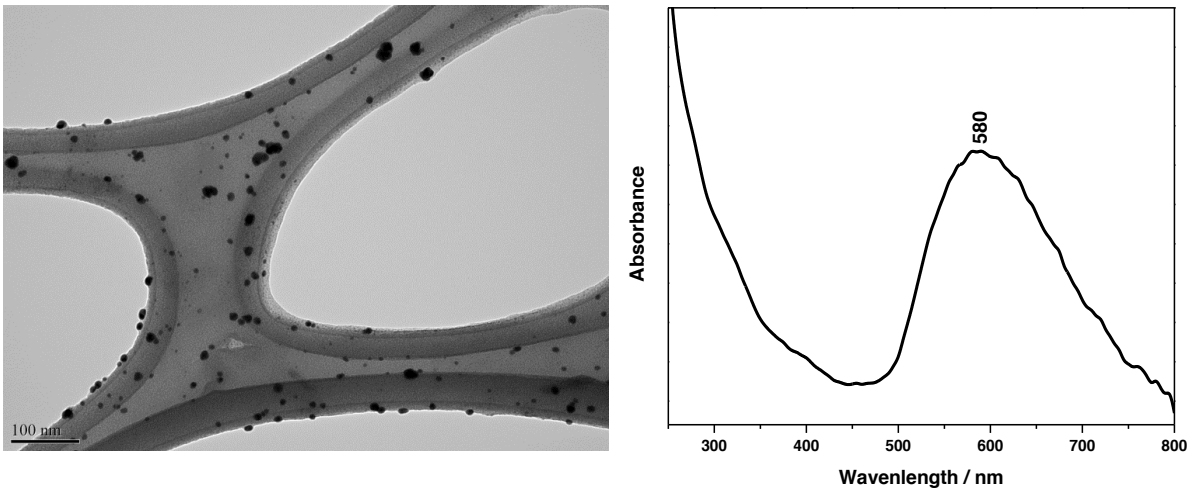

Figure 15. TEM image of TOC Au nanoparticles (135, 000 x) and corresponding UV-vis spectrum of the colloids.

It was easily discerned from the TEM image that the nanoparticles did not have a well-defined truncated octahedral shape, as was reported by Li and Ma [67]. However, for practical purposes, they will continue to be referred to as TOC AuNPs in this work. Nevertheless, the nanoparticles were 11 ± 4.1 nm, which is close to the expected size of 16 nm [67]. The unexpected shape of these nanoparticles may be related to the molar

ratio of PDDA and $HAuCl_4$, as this was found to be the key factor in the size and morphology of the Au nanostructures [67]. Reportedly, at lower PDDA concentrations, the size of the nanoparticles decreases and their shape becomes more irregular [67]. Adsorption of the PDDA onto the glass of the reaction flask may have lowered the concentration in solution. The adsorption of PDDA onto the flask was revealed when aqueous $AgNO_3$ was heated in the same flask, and a silver mirror formed. Further evidence that the synthesis carried out produced slightly different structures than those reported in the literature was that the λ_{max} of 580 nm in the UV-vis spectrum deviated from the published value of 530 nm [67].

4.6.2 SERS 4,4'-Byp on Treated Fabric

Fabric samples were treated by incubation, deposition, and *in situ* synthesis of the aforementioned colloids, to achieve a surface roughness that would render the textiles SERS-active. It has been reported that *in situ* generation of AgNPs within textile materials is particularly efficient [74]. This *in situ* process involves the adsorption of Ag^+ ions onto the fibers by electrostatic or Van der Waals forces, followed by the reduction of the silver into AgNPs [74]. The SERS spectrum of 4,4'-byp was collected on all treated samples, to evaluate their SERS activity. A 532 nm and 780 nm excitation wavelength was determined to be most effective for studies performed on silver and gold, respectively (Figure A-2).

4.6.2.1 Citrate-Reduced Silver Colloids

Citrate-reduced silver colloids were used to modify the fabric samples by incubation, deposition, and *in situ* methods. On each of the treated fabric samples, 4,4'-byp was deposited and a SERS spectrum was collected.

Figure 16 shows ten SERS spectra of 4,4'-byp collected on the fabric sample modified by incubation in the AgNP colloids.

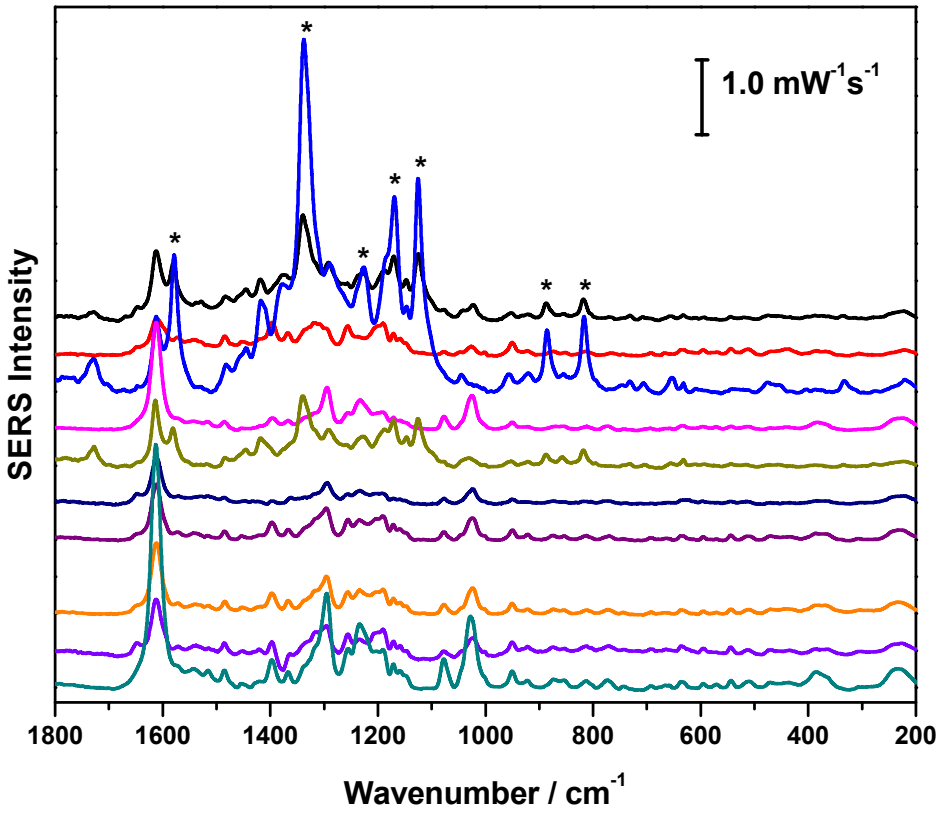

Figure 16. SERS signal of 4,4'-byp on fabric sample after incubation in citrate-reduced Ag colloids (532 nm, 10 mW, 60 s).

These spectra revealed that the signal was highly variable on the fabric, which indicated that the surface was not uniform. In most spectra, strong Raman bands at 1610, 1293, and 1000 cm^{-1} were present. This said, peaks corresponding to silk, shown by an asterisk,

were present in varying degrees in all spectra. Silk was therefore recognized as an interference for collecting the SERS signal of an analyte, and must be reduced or eliminated entirely for the fabric to be considered a viable SERS substrate. This could be achieved by roughening the metal-coating on the fibers, by increasing the density of the nanoparticles on that surface, or by covering the silk completely with nanoparticles, so that it may also be SERS-active. In this latter case, nanoparticles, if at high enough density, could also serve to block the Raman signal of silk.

The deposition of 20 μL AgNP "paste" on the fabric, certainly increased the density of the AgNPs on the fabric surface, as it was of much higher concentration than the aqueous colloid solution from which it was prepared. Figure 17 shows the 4,4'-byp SERS signal on this substrate at ten different spots on the fabric.

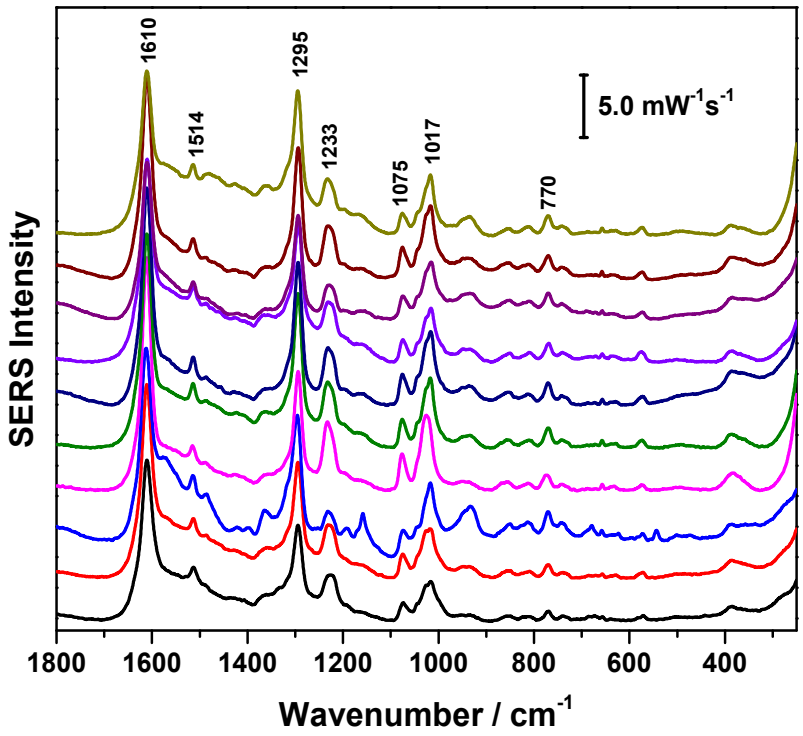

Figure 17. SERS signal of 4,4'-byp on fabric sample after deposition of citrate-reduced AgNP paste (20 μL), collected with the 532 nm laser, at 1 mW for 40 s, by Marwa Yasmin.

The spectra in Figure 17 show that the 4,4'-byp SERS signal was significantly improved from that obtained on fabric incubated in AgNPs (Figure 16), because the silk interference was almost entirely suppressed. The SERS signal appeared to be relatively uniform, however background was present in most of the spectra.

Another method of treating the fabric was pursued, in an effort to further reduce background in the SERS signal and to increase signal intensity. *In situ* synthesis of citrate-reduced AgNPs on the fabric appeared to provide better coverage of the fabric than a simple incubation and deposition of the AgNP paste. Figure 18 shows ten SERS spectra of 4,4'-byp collected on this surface. An SEM image collected of this surface is also shown in Figure 18.

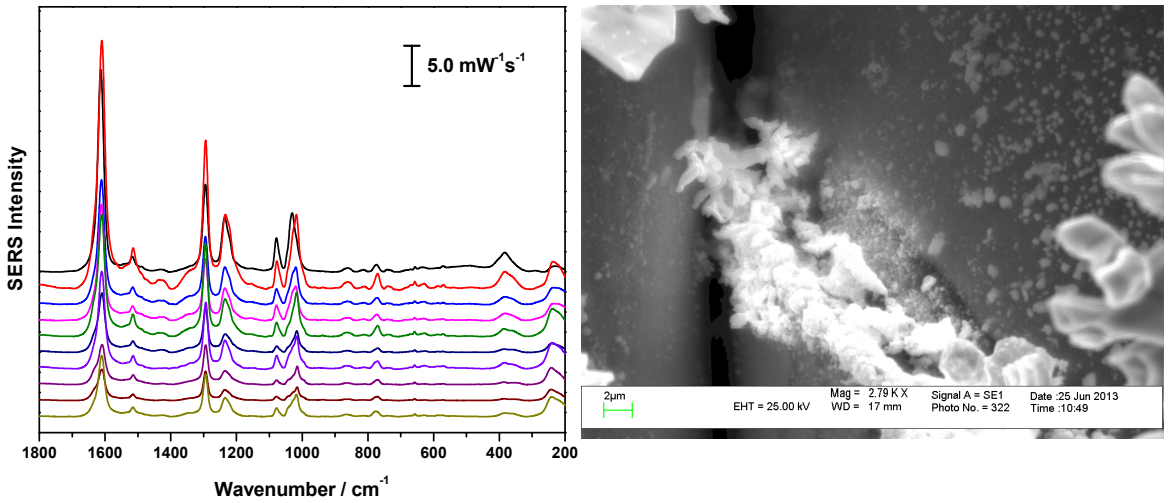

Figure 18. SERS signal of 4,4'-byp on fabric sample after *in situ* synthesis of citrate-reduced Ag colloids (10 mW, 60 s) and a high resolution SEM image of the fabric sample. The image depicts the high concentration of nanoparticles in the gap of the metal coating.

As can be observed in the SERS spectra, the signal for 4,4'-byp was very uniform, with only slight variances in peak intensities. Any interference from silk was absent. The SEM image revealed that nanoparticles coated the metal surface wrapped around the silk fibers, but more importantly, high concentrations of nanoparticles formed in the gaps between the metal coating. Therefore, the silk was completely shielded, in addition to being rendered SERS-active. The SEM image also showed that large silver crystals formed on the surface of the metal. This is due to the spontaneous redox reaction between copper and silver:

$$Cu\,(s) + 2\,Ag^{+}(aq) \rightarrow Cu^{2+}\,(aq) + 2\,Ag\,(s) \qquad (3)$$

In a separate experiment, the effect of the silver crystals on the SERS signal was examined. Two fabric chips were immersed in the aqueous $AgNO_3$ solution for longer than usual, approximately 10 minutes, prior to adding the reducing agent. This allowed significant silver crystals to coat the fabric samples (Figure A-3). Once the *in situ*

synthesis was complete, the samples were allowed to dry. The silver crystals on one fabric chip were removed by simple scraping, whereas the crystals on the other sample were left untouched. SERS of 4,4'-byp were then collected on the two substrates. A comparison of the signal collected on these surfaces is shown in Figure 19.

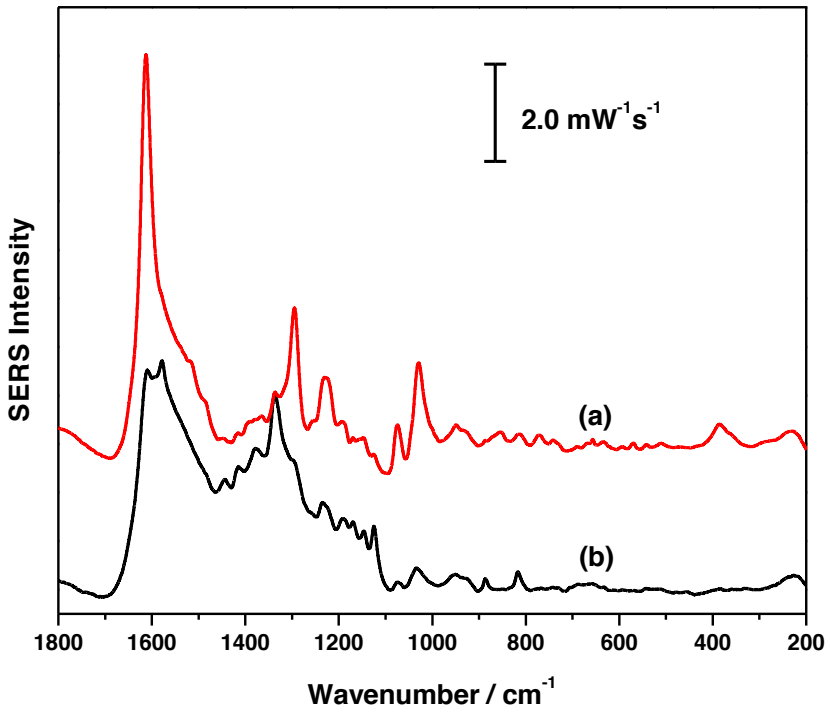

Figure 19. SERS signal of 4,4'-byp on fabric chip treated by *in situ* synthesis of AgNPs (a) with removal of silver crystals (average of 10 spectra) (b) without removal of silver crystals (average of 5 spectra), collected by 532 nm excitation, at 10 mW, for 40 s.

The SERS signal of 4,4'-byp suggests the silver crystals affected the quality of the substrate, by decreasing the Raman enhancement. This is because the crystals are too large to contribute to the SERS effect. For future work, it was critical that fabric samples were added to the aqueous solution only minutes preceding the reduction process.

4.6.2.2 Modified Citrate-Reduced Silver Nanoparticles

The SERS spectrum of 4,4'-byp was first collected on a sample treated by incubation of modified citrate-reduced AgNPs, as shown in Figure 20.

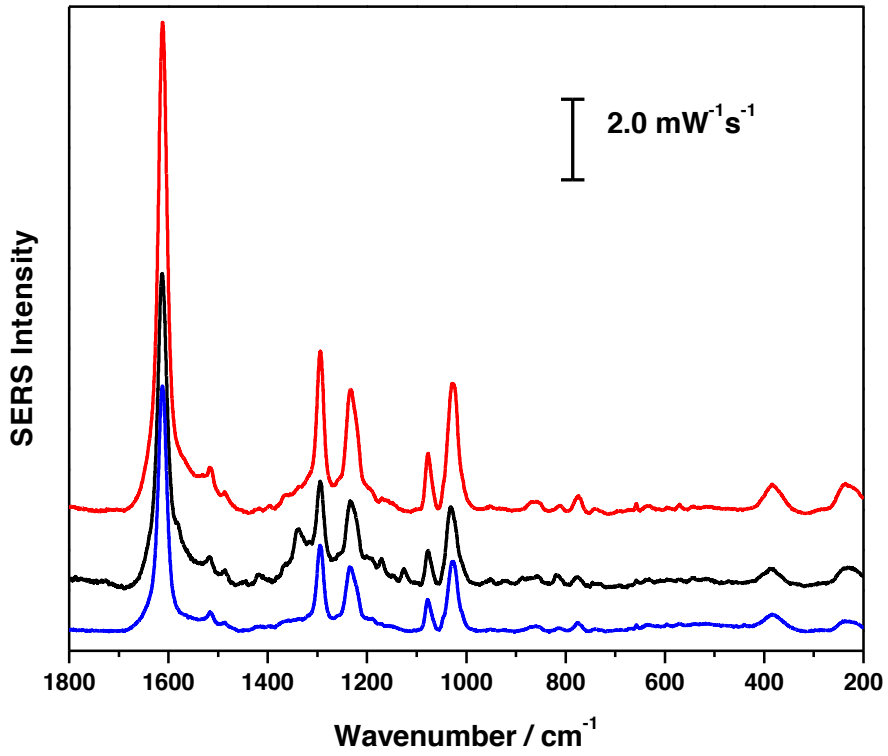

Figure 20. SERS spectra of 4,4'-byp (0.1 M) on three different spots of fabric chip incubated in modified citrate- reduced AgNPs (532 nm, 5 mW, 60 s).

From Figure 20, it was evident that the modified citrate-reduced colloids provided a much better substrate than the regular citrate-reduced AgNPs, as no silk signal was observed in the SERS spectra, unlike in Figure 16. Also, the signal intensity shows that this fabric provided good enhancement of the analyte signal. Despite this result being satisfactory, an *in situ* synthesis was pursued. Ten SERS spectra of 4,4'-byp collected on fabric after *in situ* synthesis of modified AgNPs are shown in Figure 21 *A*.

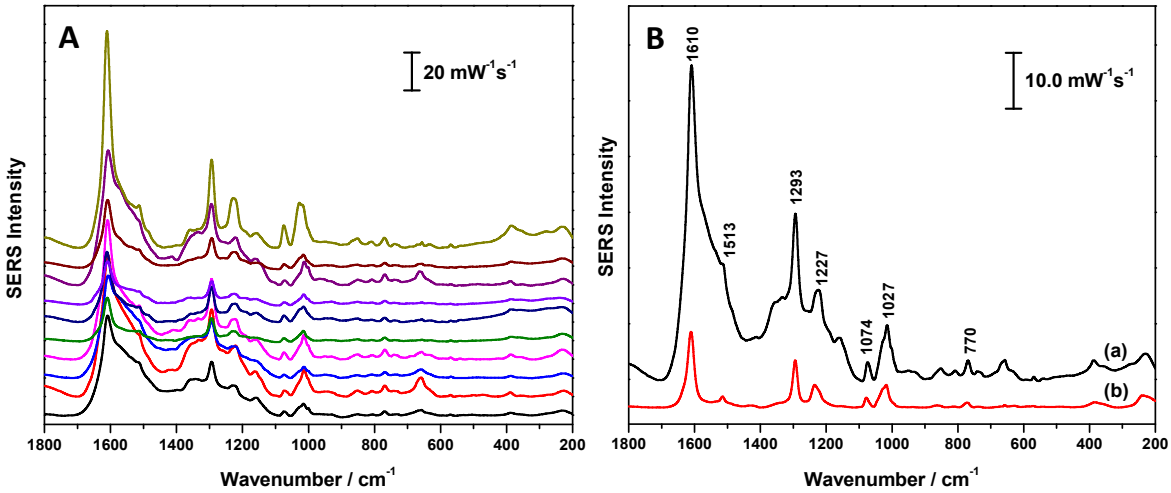

Figure 21. (A) SERS spectra of 4,4'-byp collected on a fabric chip after *in situ* synthesis of modified AgNPs (532 nm, 5 mW, 40 s) and (B) comparison of the average SERS signal collected on fabric after *in situ* synthesis of (a) modified citrate-reduced AgNPs and (b) regular citrate-reduced AgNPs.

From the ten SERS spectra collected on the fabric chip, it was noted that the spectra contained background, and the peak intensities varied significantly depending on where the laser was focused. This indicated that the substrate is not uniform. Nonetheless, it was important to consider the considerable enhancement of the 4,4'-byp signal on the fabric after treatment via *in situ* synthesis of modified citrate-reduced AgNPs. Even in comparison with the *in situ* synthesis of the regular citrate-reduced AgNPs, as shown in Figure 21 *B*, the signal intensity was considerably greater. Additionally, all the peaks for 4,4'-byp were present in the spectrum, so the spectral background did not significantly compromise detection of the analyte. This experiment was repeated in triplicate and provided reproducible results (not shown).

In another study, a second *in situ* method was explored, in which the fabric sample was added to the solution at the same time as the $NaBH_4$. From the detection of 4,4'-byp on these surfaces, it was determined that greater SERS enhancement was

achieved when the fabric was added prior to the addition of $NaBH_4$ (data not shown). It is suspected that when the fabric was added at the same time as the $NaBH_4$, silver ions did not have time to adsorb to the fabric prior to the reduction process, and therefore fewer AgNPs were formed throughout the fabric.

4.6.2.3 Silver Microspheres with Nanofeatures

Fabric samples were treated with Ag microspheres by incubation, deposition, as well as *in situ* synthesis. Firstly, solutions of Ag microspheres suspended in 4,4'-byp (0.1 M) solution were deposited on fabric chips. Figure 22, shows the SEM images of these fabric surfaces, after deposition of varying concentrations of Ag microspheres.

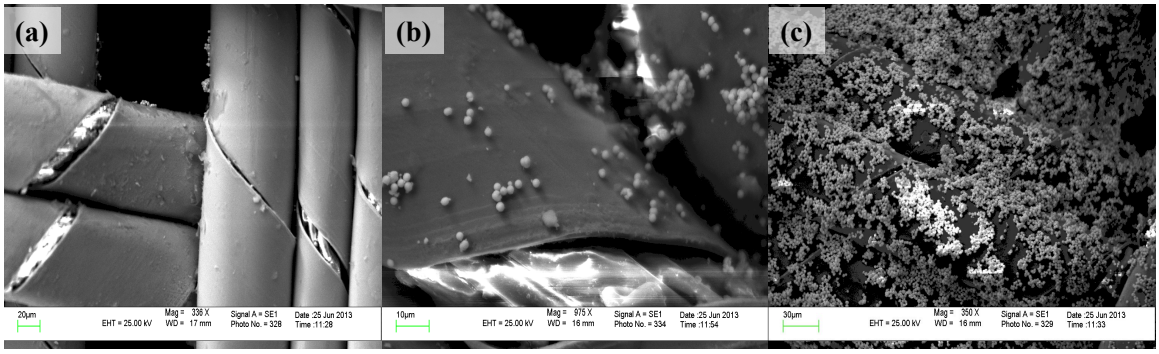

Figure 22. SEM image of fabric after a 24 hour incubation in (a) 10 mM, (b) 50 mM, and (c) 100 mM Ag microsphere solution in 4,4'-byp (0.1 M).

The fabric treated with 10 mM and 50 mM Ag microsphere solutions did not appear to be evenly coated with the silver structures. For this reason, it was anticipated they would not provide a good SERS signal of 4,4'-byp. The fabric sample treated with a 100 mM Ag microsphere solution however appeared to be uniformly covered in microspheres. The SERS spectrum of each surface was collected. These spectra are displayed in Figure 23. The SERS spectrum of an additional fabric sample that was not imaged by SEM, on which a 200 mM Ag microsphere solution was deposited, is also shown in Figure 23.

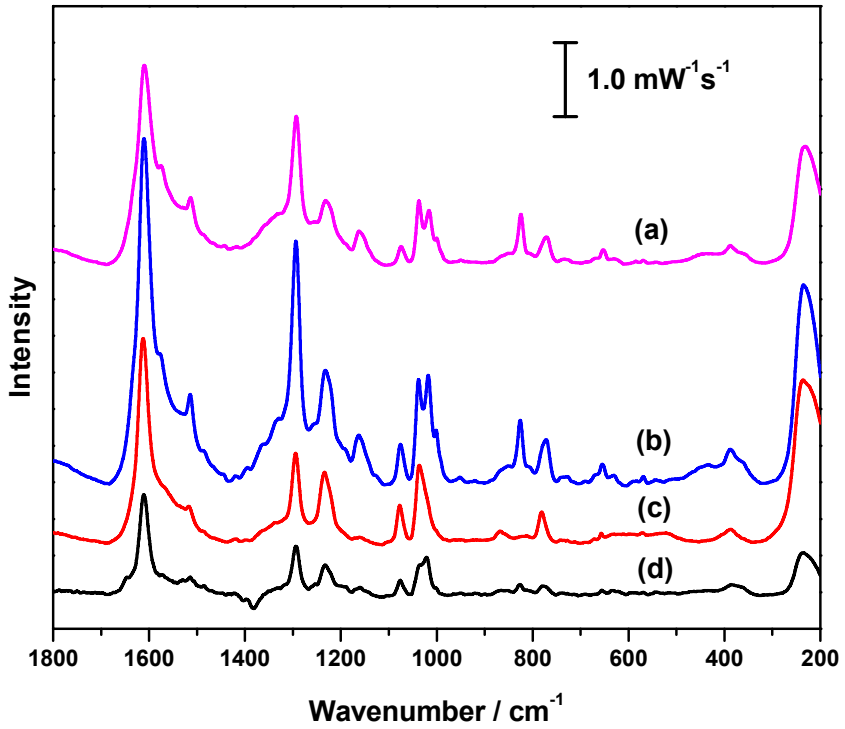

Figure 23. SERS spectra, representing the average of 10 different spots of a fabric sample after deposition of a 0.1 M 4,4'-byp solution containing (a) 200 mM (532 nm, 10 mW, 40 s), (b) 100 mM, (c) 50 mM, and (d) 10 mM Ag microsphere powder (532 nm, 10 mW, 60 s).

The spectra revealed that all fabric chips treated by deposition of Ag microspheres were SERS-active, and exhibited the most prominent bands for 4,4'-byp (1600, 1293, 1000 cm^{-1}). This said, there was a significant increase in signal intensity as the concentration of the Ag microspheres in solution was increased, up until 100 mM. The SERS spectrum of the deposition of a 200 mM solution of Ag microspheres on the fabric was weaker than that collected on the fabric treated with a 100 mM solution, but comparable to the sample treated with a 50 mM solution. This could be due to overlapping of the microspheres, creating layers on the fabric surface if the concentration of Ag structures is too high, in turn rendering the roughness of the surface uneven. It is shown however, that when an incubation of the fabric was performed in Ag microspheres, the 200 mM solution provided a greater enhancement of the 4,4'-byp signal. This is shown in Figure 24.

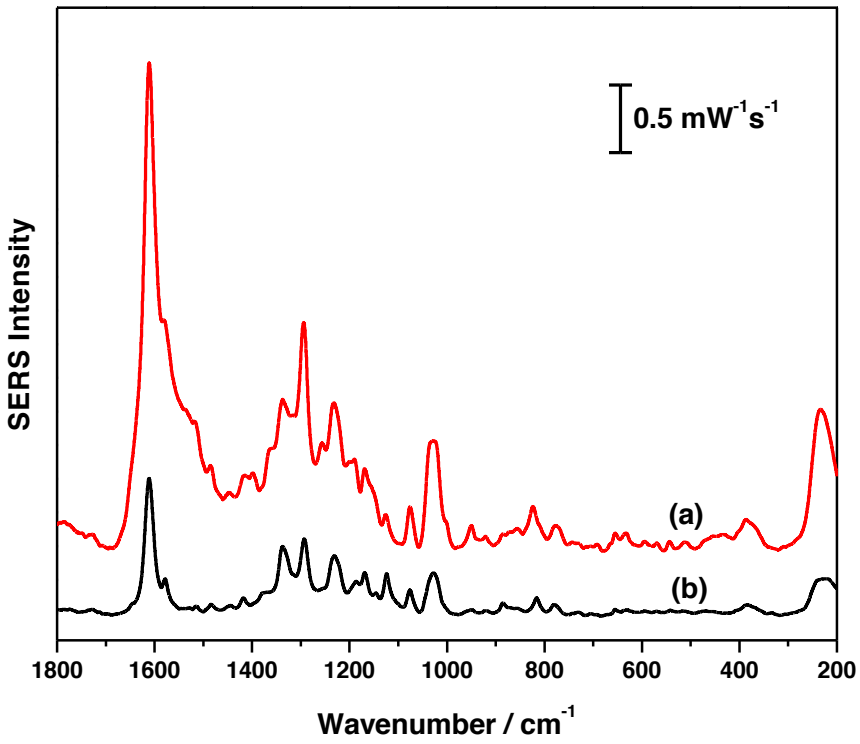

Figure 24. (a) Average SERS spectrum of 4,4'-byp (0.1 M) of 10 spots collected on fabric after a 1 hour incubation in 200 mM Ag microspheres (532 nm, 5 mW, 40 s) and (b) average SERS spectrum of 4,4'-byp (0.1 M) of 5 spots collected on fabric after a 1 hour incubation in 100 mM Ag microspheres (532 nm, 10 mW, 60 s).

The SERS signal of 4,4'-byp on fabric, after incubation in Ag microsphere solution, was affected by the SERS signal of silk, which appeared as noise in the spectra (Figure 24). This was undesirable, as previously stated, because increased noise contributes to the irreproducibility of SERS spectra.

An *in situ* synthesis of the microspheres was attempted next. The resulting microspheres were imaged by SEM, as shown in Figure 25.

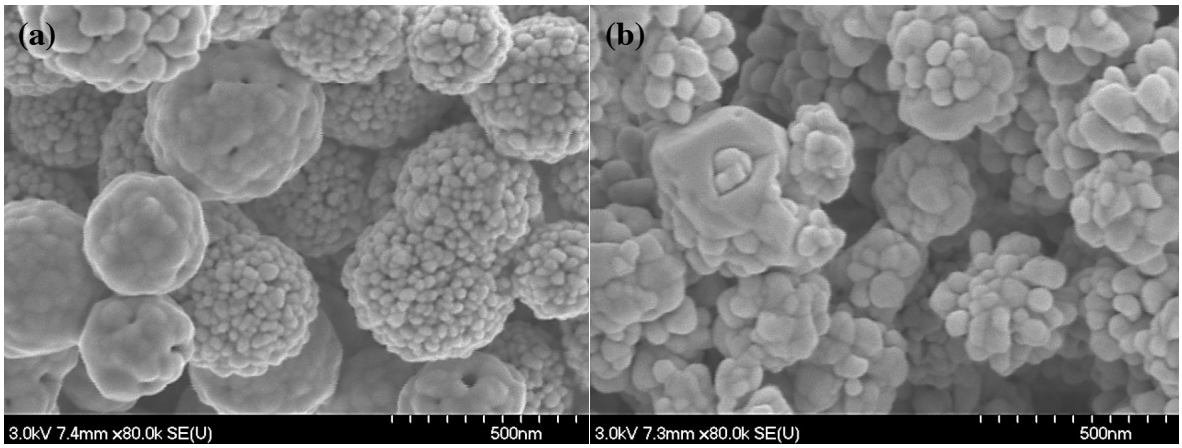

Figure 25. SEM images of Ag microspheres resulting from *in situ* synthesis (a) on a metal-coated fabric sample and (b) after washing and drying.

The SEM images revealed that the Ag microspheres were irregularly shaped and did not resemble those synthesized in the absence of the fabric chip. This may have been due to the partial reaction of the Ag^{+} with the copper in the metal-coating of the fabric, as previously discussed. This would have altered the molar ratios of the reagents, which translated to variability in the morphology of the silver structures. Although it was expected that the observed irregularity in shape of the Ag microspheres would compromise the SERS signal of 4,4'-byp, Figure 26 shows that an overall increase in signal was observed for these substrates, in comparison to an incubation in 200 mM Ag microsphere solution.

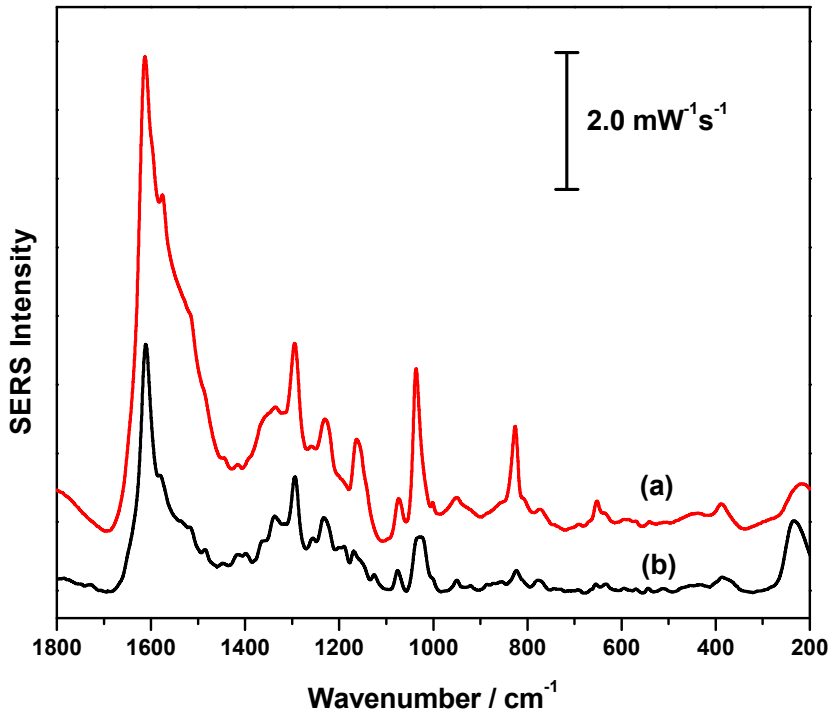

Figure 26. Average SERS spectrum of 4,4'-byp (0.1 M) of 10 spots collected on the fabric sample after (a) *in situ* synthesis of Ag microspheres (532 nm, 7 mW, 40 s), and (b) incubation in 200 mM Ag microsphere solution (532 nm, 5 mW, 40 s).

The increase in signal intensity and reduced noise in the SERS spectrum of 4,4'-byp on the fabric sample treated via *in situ* synthesis of the Ag microspheres, suggested better coverage of the fabric surface was achieved. This surface may have been less uniform on the nanoscale, but more uniform on the microscale, and this seems to have provided an important result. The signal enhancement on these substrates suggested they would be effective SERS substrates, because the detection of analytes found at trace levels is one of the goals of this work.

4.6.2.4 Gold Nanoparticles

The SERS spectrum of 4,4'-byp on a fabric sample following incubation in citrate-reduced AuNPs is shown in Figure 27.

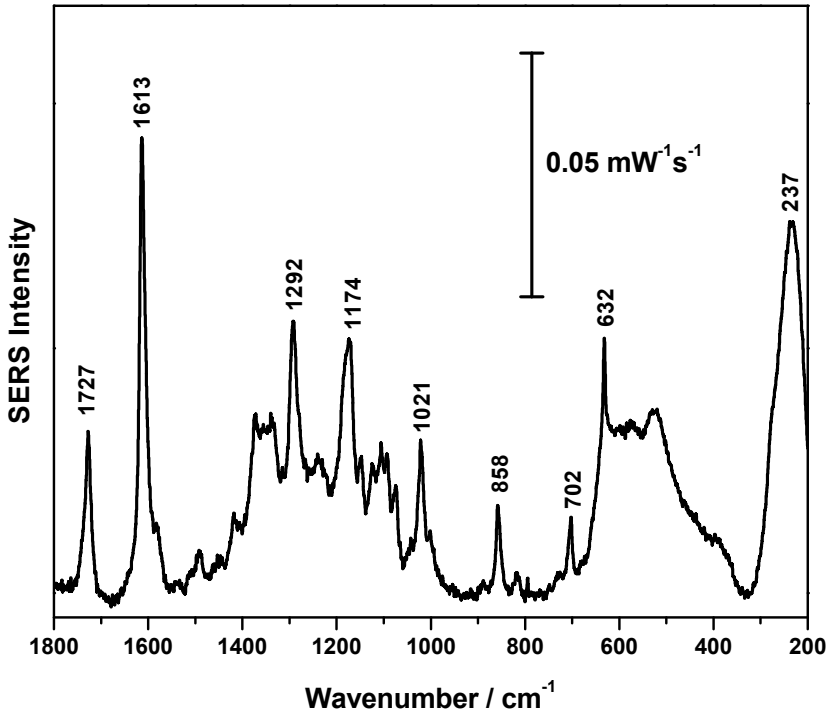

Figure 27. Average of three SERS spectra for 4,4'-byp (0.1 M) collected on a fabric sample after a 1 hour incubation in AuNPs. 785 nm laser power, at 80 mW, with a collection time of 60 s.

This spectrum was very noisy and weak. This was in part due to the nature of the metal, as gold is known to provide average enhancements, which are lower than those of silver [79]. Much of the noise in the spectrum was a result of overlapping with the silk signal. The bands at 1727, 1174, and 632 cm^{-1} in the spectrum were due to silk. Better coverage of the fabric surface by nanoparticles was therefore critical. The signal intensity was also very low, and could be improved.

One way of increasing the SERS enhancement of gold is to alter the shape of the nanoparticles, since the creation of edges and tips can concentrate the electromagnetic field onto specific regions of the nanoparticle surface [80]. In some cases, the enhancement factor on gold can be increased from 10^4 to 10^{10} just from shape change [80]. The synthesis of gold nanoshapes was therefore pursued.

4.6.2.5 Gold Nanostars

Fabric samples were treated with gold nanostars. As previously discussed, the seed-mediated synthesis of the nanostars provided inconsistent colloids, which was reflected by the significantly different λ_{max} values of different batches. The SERS spectra of 4,4'-byp was collected on fabric samples incubated in Au nanostars, as shown in Figure 28.

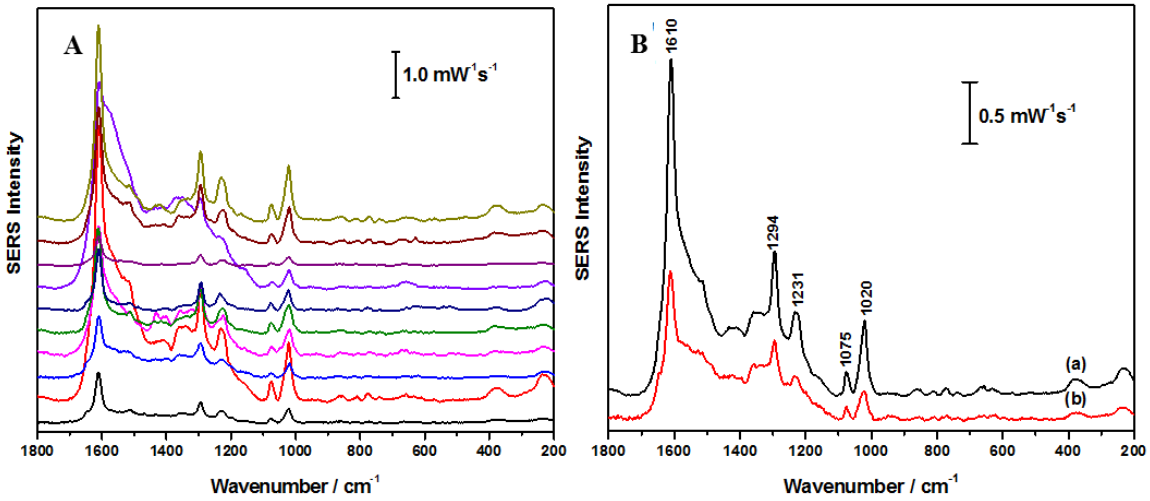

Figure 28. SERS spectrum of 4,4'-byp (0.1 M) on fabric chip after a 1 hour incubation in gold nanostars. (A) Ten spectra collected at different spots on fabric shows ($\lambda_{max\ Au\ nanostars}$ = 665 nm, 10 mW, 60 s) (B) Average 4,4'-byp signal obtained on fabric treated with Au nanostars having a λ_{max} at (a) 665 nm, and (b) 872.9 nm (average of 2 spectra, 532 nm, 10 mW, 40 s).

SERS spectra in Figure 28 *A* contained a bit of background, although the enhancement of the 4,4'-byp signal was significant in comparison to spectra collected on citrate-reduced AuNPs (Figure 27). Also, silk peaks were not observed. The main disadvantage associated with this method of preparing SERS-active substrates resided in its irreproducibility. Figure 28 *B* shows that when the λ_{max} of the colloids varied, meaning the shape and size of the nanostars were altered, the SERS substrate was changed. It appears that colloids having a lower λ_{max} provided greater enhancement. This means that a better SERS signal arose on Au nanostars that had fewer branches and were more spherical than star-shaped [78]. Since this procedure was inconsistent, alternative Au nanoshapes were explored for SERS substrates.

4.6.2.6 Gold Nanoflowers

Similar to Au nanostars, AuNFs were synthesized and used to modify the fabric chip. Figure 29 shows a fabric sample after incubation in these colloids.

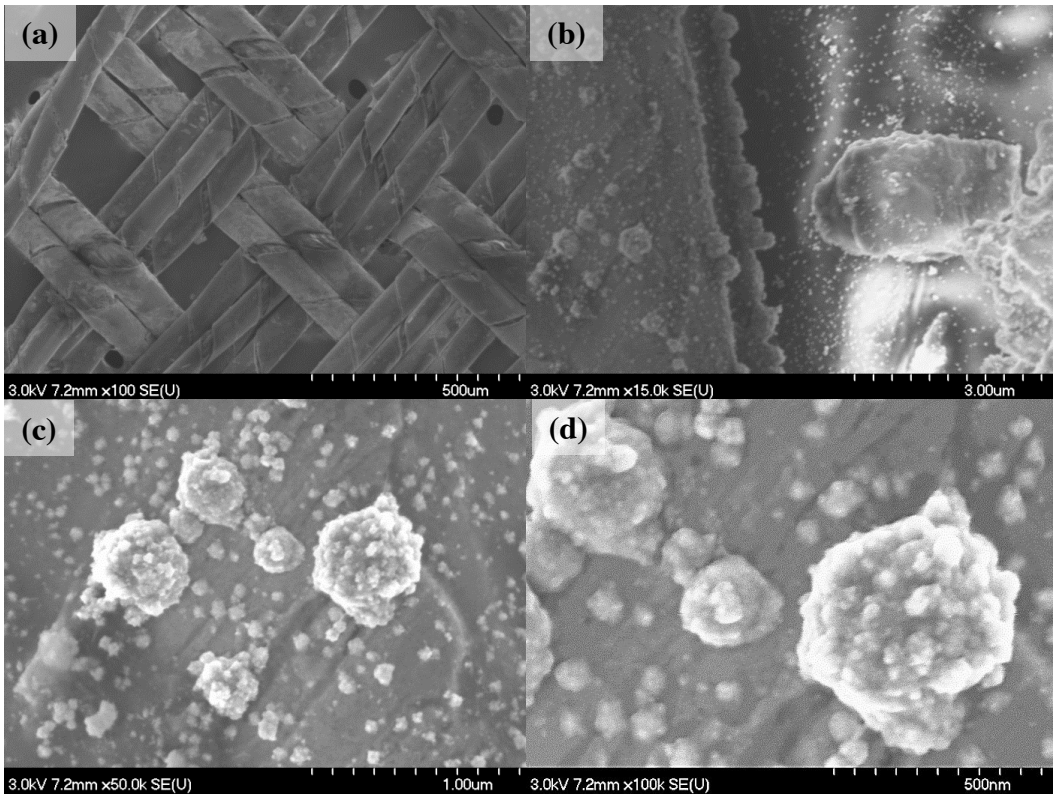

Figure 29. SEM image of fabric after incubation in AuNFs and deposition of 4,4'-byp (0.1 M) at (a,b) low magnification and (c,d) high magnification.

The SEM images revealed that the fabric sample was more or less uniformly roughened by the AuNFs, although the size of the NFs varied significantly, and larger particles ~500 nm were present. These appear to be aggregates, which formed prior to centrifugation of the colloids. The growth of the AuNFs involved the attachment of small gold particles onto the surface of the gold seeds, so if that growth was allowed to continue for longer than a few minutes, aggregates could have formed in solution [66]. Ten SERS spectra were collected on this surface (Figure 30) to examine the uniformity of the 4,4'-byp signal.

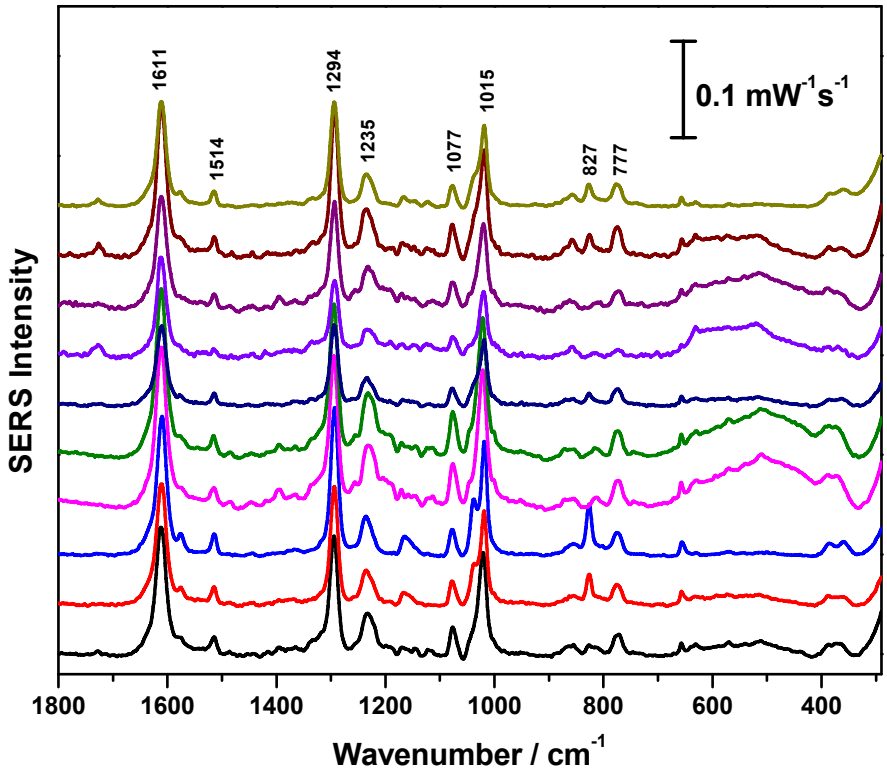

Figure 30. SERS signal of 4,4'-byp (0.1 M) at ten different spots of fabric sample after a 1 hour incubation in gold nanoflowers (780 nm, 70 mW, 40 s).

The SERS spectra showed that this surface provided a steady signal; peak intensities were relatively consistent and signal was free from background interferences. This experiment was repeated in triplicate, and demonstrated good reproducibility. Due to the uniformity of the SERS signal on this substrate, this method of treatment could be used to produce substrates with the potential applications for quantitative studies.

4.6.2.7 Truncated Octahedral (TOC) Gold Nanoparticles

The SERS signal of 4,4'-byp was monitored on a fabric chip after incubation in TOC AuNPs. These spectra are presented in Figure 31.

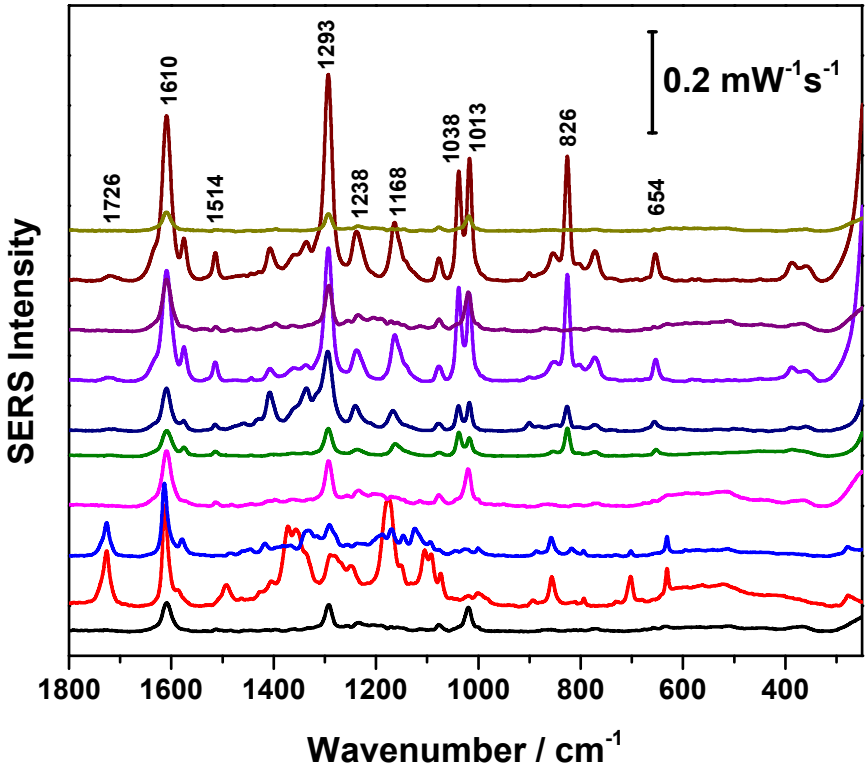

Figure 31. SERS spectra of 4,4'-byp (0.1 M) at 10 different spots on a fabric sample after a 1 hour incubation in truncated octahedral nanoparticles (780 nm, 100 mW, 50 s).

The SERS spectra revealed that silk interfered with the signal and that the signal was highly inconsistent across the fabric chip, as the peak intensities varied significantly in different spots. This method showed that incubation in the TOC nanoparticles was not useful for the creation of a reliable SERS-active substrate.

4.6.3 Detection of Biomolecules on Treated Fabric

Based on the SERS data of 4,4'-byp collected on various fabric samples treated with NPs, it was determined that the substrates demonstrating the most potential for the detection of bioanalytes were fabric chips after *in situ* synthesis of modified citrate-reduced AgNPs and Ag microspheres, as well as after incubation in AuNFs. The latter

was noted as a reliable substrate, not because of its signal enhancement, as in the case of fabrics treated with Ag, but rather because the 4,4'-byp signal was most consistent. This is an important factor, if the substrate is to be used for quantitative studies.

As previously stated, 4,4'-byp is a strong Raman scatterer, whereas many biomolecules are weak Raman scatterers. It was imperative that the detection of a biomolecule be attempted on the modified fabric samples, as a proof-of-concept for the monitoring of biomarkers. Guanine and its derivatives guanosine and dGMP, whose structures are shown in Figure 32, were selected as analytes due to their structural similarities to 8-oxo-2'-deoxyguanosine, Figure 32 *d*, a biomarker for oxidative stress.

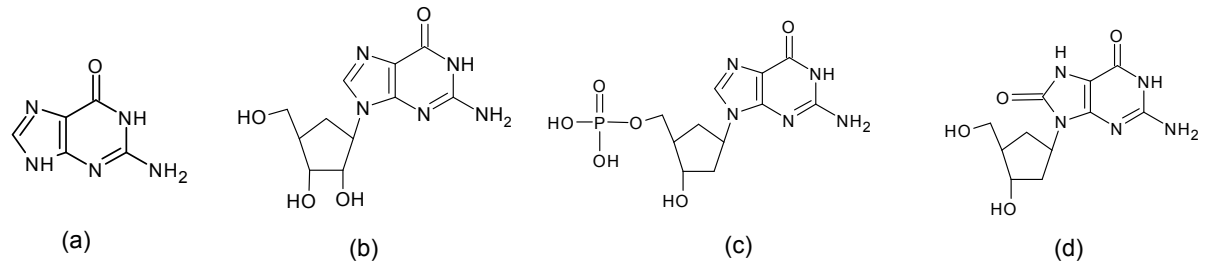

Figure 32. Molecular structure of (a) guanine, (b) guanosine, (c) 2'-deoxyguanosine-5'-monophosphate, and (d) 8-oxo-2'-deoxyguanosine.

Oxidative stress is a physiological condition that arises when an imbalance exists between reactive oxidative species and natural antioxidant enzymes [81]. This means that oxidative stress is associated with numerous physiological conditions including aging, atherosclerosis, hypertension, renal failure, immune alterations, neurodegeneration, diabetes, radiation damage, cancer, and exposure to toxins, such as heavy metals and pesticides [81, 82, 83].

The normal Raman signal of dGMP shows numerous characteristic peaks, as shown in Figure 33. Complete band assignment is provided in Table A-3.

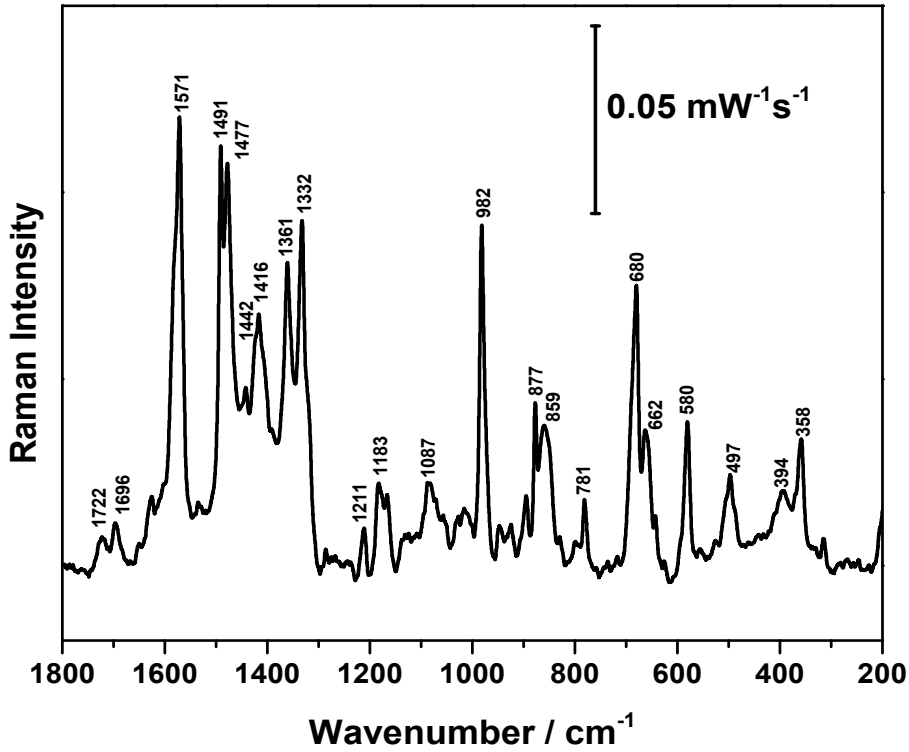

Figure 33. Normal Raman spectrum of pure dGMP powder (532 nm laser, 7 mW, 40 s).

dGMP displayed many bands in the region between 1330-1600 cm^{-1}, which could overlap or be confused with silk bands, if detected on fabric. Bands at 982 and 680 cm^{-1} are unique to dGMP, however, and could be used to identify the presence of this analyte on the SERS substrates.

An attempt was made at collecting a SERS spectrum of dGMP on a fabric sample after *in situ* synthesis of modified citrate-reduced AgNPs, however the silk signal dominated the spectrum. This result was unexpected, as this method had previously provided excellent coverage of the fabric, and presumably the silk. Another possibility for this result was the presence of the low scattering cross sections of the sugar and phosphate group bound to the base, which essentially diluted the observed SERS signal [84]. Furthermore, the concentration of dGMP in solution was quite low, and in solution,

nucleotides are generally considered to be deprotonated, with the two non-bridging oxygen atoms of the phosphate group carrying a negative charge [85]. This could compromise the adsorption of dGMP onto the surface of the AgNPs, since citrate was already present on the surface of the AgNPs, and also carried a negative charge. dGMP may not have been able to displace the citrate molecules, and since SERS is distance-dependent, only a very weak signal could be observed.

When the SERS of dGMP was collected on fabric treated by *in situ* synthesis of Ag microspheres, other issues arose. In this case, no citrate was present, however since the Ag microspheres could not be washed, ascorbic acid and potassium biphthalate contaminated the fabric (Figures A-4, A-5, A-6). dGMP, unlike 4,4'-byp, could not displace these compounds from the metal surface. As a result, no dGMP could be detected.

The spectrum of dGMP was collected on a fabric sample after incubation in AuNFs. This spectrum presented three peaks (1418, 1333, and 794 cm^{-1}) that possibly correspond to dGMP. However, these bands were very weak and the spectrum was dominated by the silk signal (Figure A-7).

As of yet, the detection of guanosine on the fabric substrates has also been unsuccessful. This is possibly due to the poor adsorption of this molecule on the metal surface. It is expected that electrostatic adsorption would be the mechanism by which it is held on the metal surface, therefore citrate and other contaminants would greatly affect adsorption of guanosine onto the metal, resulting in poor SERS analysis.

In comparison to dGMP and guanosine, guanine has a strong Raman signal, as shown in Figure 34. Complete band assignment is provided in Table A-3.

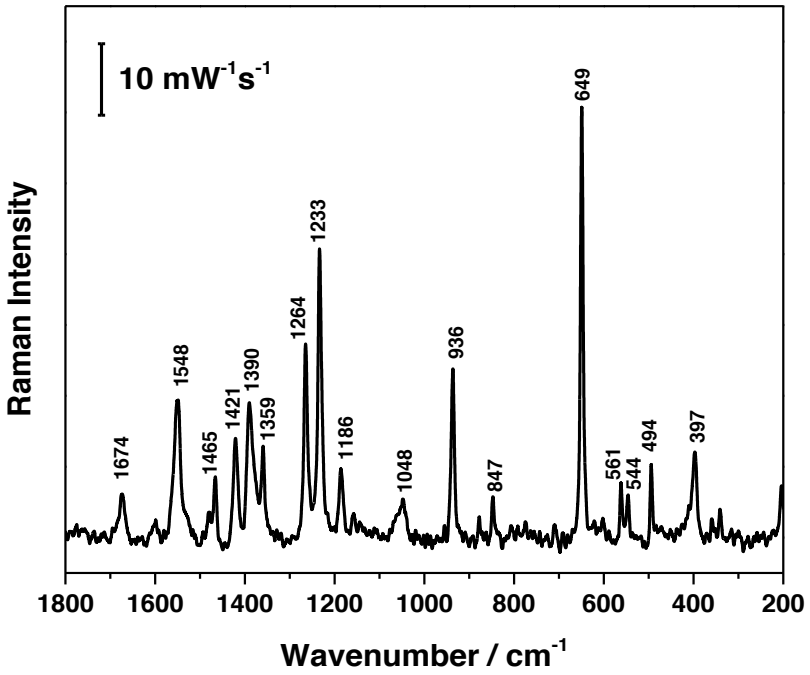

Figure 34. Normal Raman spectrum of pure guanine powder (532 nm, 5 mW, 10 s).

This base was unsuccessfully detected on the fabric SERS substrates prepared by *in situ* synthesis of nanoparticles, or by treatment in AuNFs, however a very weak signal was detected on a fabric chip after deposition of citrate-reduced AgNP paste. Ten SERS spectra of guanine were collected on this surface (Figure A-8). The average of these spectra is shown in Figure 35, alongside the SERS signal of the substrate prior to the deposition of the aqueous guanine solution.

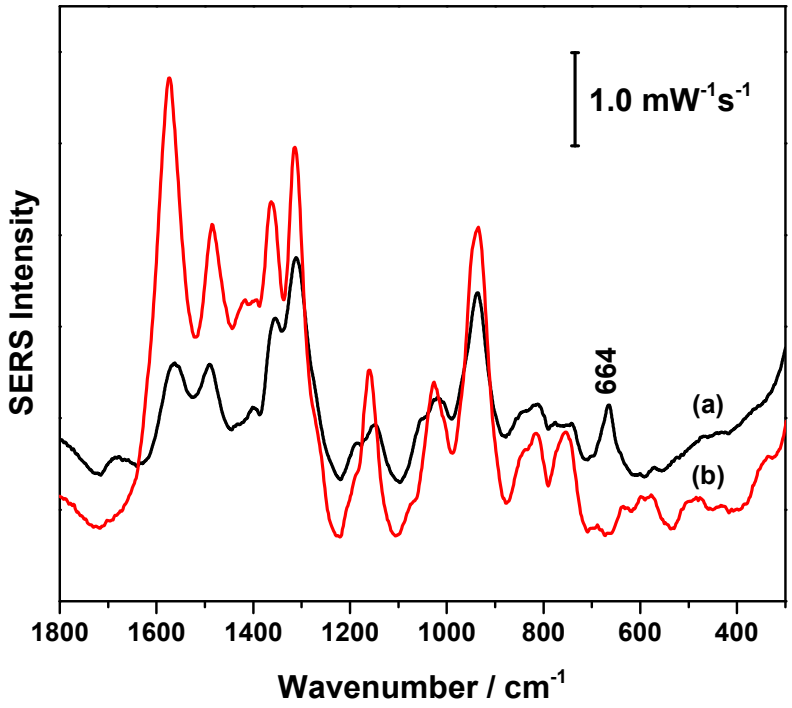

Figure 35. SERS spectrum of fabric treated by deposition of 20 μL of citrate-reduced AgNP paste (a) after deposition of aqueous guanine solution (1.0 mM, average of 10 spectra) and (b) prior to deposition of guanine (average of 10 spectra), collected with the 532 nm laser, at 2 mW for 40 s.

The comparison provided in Figure 35 showed that citrate was present on the surface of the AgNPs, and provided its own SERS signal (Figure 35 *b*). Even when guanine was deposited on the substrate, citrate dominated the SERS spectrum. However, a weak, but well-defined band at 664 cm^{-1}, characteristic of guanine, was identified in Figure 35 *a*, indicating it was present on the surface. This band could therefore be used as a marker band for guanine, although it is preferable to have a series of SERS bands for a given analyte to ensure definite identification. Interference by citrate must be eliminated to achieve better SERS spectra of biomolecules.

Chapter 5: Conclusion

5.1 Conclusion

This work outlines the fabrication of SERS substrates from metal-coated fabric, by electrochemical roughening techniques and deposition of AgNPs and AuNPs. Electrochemical treatments generated irregular surfaces, which were not suitable for SERS applications. The inconsistent roughening obtained through this method is possibly due to the nature of the metal coating on the fabric, which is an alloy, rather than a pure metal. Nevertheless, fabric samples modified by incubation, deposition and *in situ* synthesis of various silver and gold colloids created SERS substrates capable of detecting 4,4'-byp. One of the main difficulties encountered during these studies was the spectral interference of silk. In many cases, silk generated significant background in the SERS spectra and for some samples, silk bands dominated the spectrum. It was determined that if the concentration of nanoparticles was sufficiently high on the fabric, the silk signal was suppressed. *In situ* synthesis was one way of achieving a high density of nanoparticles on the fabric. In particular, the *in situ* synthesis of Ag microspheres and modified citrate-reduced AgNPs appeared to create excellent substrates, in terms of the absence of silk interference and good signal enhancement. However, this was only true when 4,4'-byp was used as the analyte. The attempt at detecting two biomolecules, dGMP and guanosine, by SERS on these substrates was unsuccessful. It was postulated that citrate present on the modified citrate-reduced AgNPs may generate an unfavourable surface charge for the adsorption of the biomolecule, which is unable to displace citrate from the metal. Furthermore, it was determined that the Ag microspheres should be washed prior to being used for fabric treatment, as the reducing agents biphthalate and

ascorbic acid are strong Raman scatterers and inhibit the analyte signal. Contrary to silver, any possible residual reagents are removed from gold colloids prior to treating the fabric via centrifugation. AuNFs provided relatively uniform SERS substrates, as the SERS signal of 4,4'-byp was consistent across their surface, though the signal enhancement was much less than on silver. As on the other substrates, the detection of dGMP and guanosine on fabric incubated in AuNFs, was unsuccessful, and instead a very strong silk signal was observed. A single SERS band was observed for guanine on a fabric chip after deposition of concentrated citrate-reduced AgNPs.

Although it appears that metal-coated fabric modified with NPs is not well suited for the detection of the chosen biomolecules, this may not be the case for all biomarkers, as dGMP and guanosine are deprotonated in alkaline solution, and all are repelled by the negative charge carried by citrate or biphthalate on the NP surfaces. It also appears guanine was unable to fully displace citrate on the surface of the fabric substrate. Further investigations surrounding the model proposed in this work must therefore be undertaken.

5.2 Future Work

The need to produce a reliable SERS substrate from metal-coated fabric persists, as the goal of developing of a SERS substrate for the detection of biomarkers, without the incorporation of lengthy procedures of sample treatment or analysis, has not yet been met. The preliminary work reported herein using the detection of 4,4'-byp, guanine and its derivatives, as a model, provided great insight into the various parameters that play a role in achieving the aforementioned goal. Two main factors that contribute to the quality of fabric SERS substrates and remain unsolved are: the elimination of interference from silk in the analyte signal and reagents that may act as contaminants on the nanoparticle

surface. For future studies, it may be worthwhile working with fabrics made of fibers other than silk, such as cotton, if available. The effect of variables, such as washing of the colloids, incubation time, nanoparticle concentration, and the time at which fabric is added to solution during *in situ* synthesis, should be independently examined for the syntheses that appear to be most promising, as reported in this work. Furthermore, another biomolecule or relevant analyte should be selected for SERS studies, as it seems guanine and its derivatives are not well suited for SERS studies. Possible compounds include the metabolites of phthalates (di-2-ethylhexyl phthalate, di-n-butyl phthalate, di-isobutyl phthalate, and benzylbutyl phthalate), which have been shown to be present in the urine of infants who have consumed products containing certain plasticizers [86]. This would provide additional insight as to the quality of the formed substrates and act as a proof-of-concept for the monitoring of biomarkers in bodily fluids.

Finally, studies aimed at examining the durability of SERS fabric-based sensors would be crucial. This would involve washing and friction studies, to imitate how clothing and other textiles may be worn and treated.

References

[1] Xu, W.; Xia, J.; Dresselhaus, M. S.; Kong, J.; Xu, H.; Liu, Z. Zhanga, J. *Proc. Natl. Acad. Sci. U.S.A*. **2012**, *109*, 9281–9286.

[2] Yager, P.; Edwards, T.; Fu, E.; Helton, K.; Nelson, K.; Tam, M. R.; Weigl, B. H. *Nature*. **2006**, *442*, 412-418.

[3] Yamamoto, Y. S.; Ishikawa, M.; Ozaki, Y.; Itoh, T. *Front. Phys*., **2014**, *9*, 31–46.

[4] Browne, R. W.; McGarvey, J. J. *Coord. Chem. Rev.* **2007**, *251*, 454–473.

[5] Zhang, X.; Yonzon, C.R.; Young, M.A.; Stuart, D.A.; Van Duyne, R.P. *IEE Proc Nanobiotechnol.* **2005**, *152*, 195-206.

[6] Simon, C.; Potter, E.; McCabe, M.; Baggerman, C. Smart Fabrics Technology Development. Johnson Space Center, Engineering Directorate, Avionics Systems Division. October 8, 2010.

[7] Choi, S.; Zhongwei, J. *Sensors and Actuators A*. **2006**, *128*, 317-326.

[8] Maetzler, W.; Domingos, J.; Srulijes, K.; Ferreira, J.J.; Bloem, B.R. *Mov Disord*. **2013**, *28*, 1628-1637.

[9] Collins, G.E.; Buckley, L.J. *Synthetic Metals*. **1996**, *78*, 93-101.

[10] Liu, R.; Wang, S.; Lao, T.T. *J. Eng. Fiber Fabr.* **2012**, *4*, 50-56.

[11] Staneva, D.; Grabchev, I.; Betcheva, R. *Dyes and Pigments*. **2013**, *98*, 64-70.

[12] Windmiller, J.R.; Wang, J. *Electroanalysis*. **2013**, *25*, 29-46.

[13] Coyle , S.; Wu, Y.; Lau, K.-T.; Brady, S.; Wallace, G.; Diamond, D. *4th International Workshop on Wearable and Implantable BSN*. **2007**, *13*, 35-39.

[14] Tamura, S.; Tsukahara,H.; Ueno, M.; Maeda, M.; Kawakami, H.; Sekine, K.; Mayumi, M. *Free Radic. Res.*, **2006**, *40*, 1198–1205.

[15] Lee, J.; Kim, J. H.; Lee, S. H.; Kim, J. Y.; Mah, S. J.; Gu, M. B. *BioChip J*. **2013**, *7*, 180-187.

[16] Chuang, M.-C.; Windmiller, J. R.; Santhosh, P.; Ramirez, G. V.; Galik, M.; Chou, T.-Y.; Wang, J. *Electroanalysis.* **2010**, *22*, 2511 – 2518.

[17] Martino, R.; Malet-Martino, M.; Gilard, V.; Balayssac, S. *Anal Bioanal Chem.* **2010**, *398*, 77-92.

[18] Wen, Z.-Q. *J. Pharm. Sci*. **2007**, *96*, 2861-2878.

[19] Ocampo, M. C. Construction, optimization and testing a coherent anti-stokes Raman scattering microscope. M.S. Thesis, The Ohio State University, OH, 2011.

[20] Kudelski, A. *Talanta.* **2008**, *76*, 1-8.

[21] Lee, P.C.; Meisel, D. J. *Phys. Chem*. **1982**, *86*, 3391−3395.

[22] Browne, W. R.; McGarvey, J. J. *Coord. Chem. Rev*. **2007**, *251*, 454-473.

[23] Campion, A.; Kambhampati, P. *Chem. Soc. Rev*. **1998**, *27*, 241-250.

[24] Stiles, P.L.; Dieringer, J. A.; Shah, N. C.; Van Duyne, R. P. *Annu. Rev. Anal. Chem*. **2008**, *1*, 601–26.

[25] McGoverin, C.M.; Rades, T.; Gordon, K. C. *Journal of Pharmaceutical Sciences*. **2008**, *97*, 4598-4621.

[26] Kumar, C. S. S. R., Ed. *UV-vis and Photoluminescence Spectroscopy for Nanomaterials Characterization*; Springer-Verlag: Berlin, Germany, 2013.

[27] Muniz-Miranda, M. et al. Fabrication of nanostructured silver substrates for surface-enhanced Raman spectroscopy. *J Nanopart Res*. **2011**, *13*, 5863–5871.

[28] Penn, M. A.; Drake, D. M.; Driskell, J. D. *Anal. Chem*. **2013**, *85*, 8609−8617.

[29] Podstawka-Proniewicz, E.; Niaura, G.; Proniewicz, L. M. *J. Phys. Chem. B.* **2010**, *114*, 5117–5124.

[30] Oo, S. Z.; Chen, R. Y.; Siitonen, S.; Kontturi, V.; Eustace, D. A.; Tuominen, J.; Aikio, S.; Charlton, M. D. B. *Optics Express*. **2013**, *21*, 18484-18491.

[31] Chang, C.-C.; Hsu, T.-C.; Liu, Y.-C.; Yang, K.-H. *J. Mater. Chem*. **2011**, *21*, 6660–6667.

[32] Zheng, J.; Li, X.; Gu, R.; Lu, T. *J. Phys. Chem. B*. **2002**, *106,* 1019-1023.

[33] Cejkova, J.; Prokopec, V.; Brazdova, S.; Kokaislova, A.; Matejka, P.; Stepanek, F. *Appl. Surf. Sci*. **2009**, *255*, 7864–7870.

[34] Liu, Y.-C.; Yu. C.-C.; Sheu, S.-F. S. *Anal. Chim. Acta*. **2006**, *577*, 271–275.

[35] Ren, B.; Liu, G.-K.; Lian, X.-B.; Yang, Z.-L.; Tian, Z.-Q. *Anal. Bioanal. Chem*. **2007**, *388*, 29–45.

[36] Kneipp, K.; Kniepp, H.; Itzkan, I.; Dasari, R. R.; Feld, M. S. *J. Phys. Condens. Matter*. **2002**, *14*, R597–R624.

[37] Guerrero-Martínez, A.; Barbosa, S.; Pastoriza-Santos, I.; Liz-Marzan, L. M. *Current Opinion in Colloid & Interface Science*. **2011**, *16*, 118–127.

[38] Jena, B. K.; Mishra, B. K.; Bohidar, S. *J. Phys. Chem. C.* **2009**, *113*, 14753–14758.

[39] Scholes, F. H.; Davis, T. J.; Vernon, K. C.; Lu, D.; Furman, S. A.; Glenn, A. M. *J. Raman Spectrosc*. **2012**, *43*, 196-201.

[40] Nery E. W.; Kubota, L. T. *Anal Bioanal Chem*. **2013**, *405*, 7573–7595.

[41] Chakraborty, I.; Bag, S.; Landman, U.; Pradeep, T. *J. Phys. Chem. Lett*. **2013**, *4*, 2769−2773.

[42] Figueroa, M. A. Fabrication of surface enhanced Raman Scattering (SERS) substrates made from nanoparticle printing inks for detection of biological molecules. Ph.D. Thesis, Drexel University, Philadelphia, PA, August 2012.

[43] Kim, K.; Lee, H. B.; Lee, J. W.; Shin, K. S. *J Colloid Inerface Sci*. **2010**, *345*, 103-108.

[44] Benedetti, D. P.; Zhang, J.; Tangue, T. J.; Lombardi, J. R.; Leona, M. *J Raman Spec*. **2014**, *45*, 123-127.

[45] Lind, H.; Wilson, J.; Mather, R. *Physica Status Solidi A*. **2011**, *208*, 2765-2771.

[46] Yang, Y.; Xia, Y.; Huang, W.; Zheng, J.; Li, Z. *J Solid State Electrochem*. **2012**, *16*, 1733–1739.

[47] Liu, Y.-C. *J. Electroanal. Chem*. **2007**, *611*, 217–224.

[48] Ahuja, S.; Jespersen, N., Eds. *Modern Instrumental Analysis.* Elsevier: Amsterdam, The Netherlands, 2006.

[49] Pennycook, S. J. A Scan through the history of STEM. In *Scanning Transmission Electron Microscopy*; Pennycook, S.J and Nellist, P. D., Eds.; Springer Science+Business Media: New York, USA, 2011; pp1-91.

[50] Stadtländer, C. T. K.-H. Scanning Electron Microscopy and Transmission Electron Microscopy of Mollicutes: Challenges and Opportunities; Méndez-Vilas, A. and Díaz, J., Eds.; Formatex Research Center: Extramadura, Spain, 2007; pp122-131.

[51] Pantelic, R. S.; Meyer, J. C.; Kaiser, U.; Stahlberg, H. *Solid State Commun*. **2012**, *152*, 1375–1382.

[52] Ayache, J. et al. *Sample Preparation Handbook for Transmission Electron Microscopy*. Springer Science+Business Media: New York, USA, 2010.

[53] Suga, M. Asahina, S; Sakuda, Y.; Kazumori, H.; Nishiyama, H.; Nokuo, T.; Alfredsson, V.; Kjellman, T.; Stevens, S. M.; Cho, H. S.; Cho, M.; Han, L.; Che, S.; Anderson, M. W.; Schuth, F.; Deng, H.; Yaghi, O. M.; Liu, Z.; Jeong, H. Y.; Stein, A.; Sakamoto, K.; Ryoo, R.; Terasaki, O. *Progress in Solid State Chemistry*. **2014**; 1-21.

[54] He, M.; Lu, T.-M. Metal-Dielectric Interfaces in Gigascale Electronics-Thermal and Electrical Stability. Springer Science+Business Media: New York, USA, 2012.

[55] Carlton, R. A. Pharmaceutical Microscopy. Springer Science+Business Media: New York, USA, 2011.

[56] Kalantar-zadeh, K. *Sensors-An Introductory Course*. Springer Science+Business Media: New York, USA, 2013.

[57] Faulds, K.; Hernandez-Santana, A.; Smith, W. E. *Spectrosc. Prop. Inorg. Organomet. Compd*. **2010**, *41*, 1–21.

[58] Robinson, A. M.; Harroun, S. G.; Bergman, J.; Brosseau, C. L. *Anal Chem.* **2012**, *84*, 1760-1764.

[59] Ko, C. K.; Lee, W. G. S*urf. Interface Anal.* **2010**, *42*, 1128–1130.

[60] Kudelski, A.; Bukowska, J.; Janik-Czachor, M.; Grochala, W.; Szummer, A.; Dolata, M. *Vib. Spectrosc*. **1998**, *16*, 21-29.

[61] Lee, P.C.; Meisel, D. J. *Phys. Chem*. **1982**, *86*, 3391−3395.

[62] Zhao, L.; Ding, K.; Ji, X.; Li, J.; Wang, H.; Yang, W. *Colloids and Surfaces A: Physicochem. Eng. Aspects*. **2011**, *386*, 172–178.

[63] Huang, Q.; Zhu, X. *Mater. Chem. and Phys*. **2013**, *138*, 689-694.

[64] Ji, X.; Song, X.; Li, J.; Bai, Y.; Yang, W.; Peng, X. *J. Am. Chem. Soc.* **2007**, *129*, 13939–13948

[65] Yuan, H.; Fales, A. M.; Khoury, C. G.; Liu, J.; Vo-Dinh, T. *J. Raman Spectrosc*. **2013**, *44*, 234-239.

[66] Zhao, L.; Ji, X.; Sun, X.; Li, J.; Yang, W.; Peng, X. *J. Phys. Chem. C*. **2009**, *113*, 16645-16651.

[67] Li, Y.; Ma, Z. *Nanotechnology*. **2013**, *24*, 1-7.

[68] Zhuang, Z. Cheng, J. B.; Wang, X.; Zhao, B.; Han, X. X.; Luo, Y. L. *Vib. Spectrosc*. **2009**, *49*, 118–123.

[69] Zhuang, Z. Cheng, J.; Wang, X.; Zhao, B.; Han, X.; Luo, Y. *Spectrochimica Acta Part A*. **2007**, *67*, 509–516.

[70] Monti, P.; Freddi, G.; Tsukada, M.; Bertoluzza, A.; Asakura, T. *J. Raman Spectrosc.* **2001**, *32*, 103–107.

[71] Rousseau, M.-E.; Lefevre, T.; Beaulieu, L.; Asakura, T.; Pezolet, M. *Biomacromolecules*. **2004,** *5*, 2247-2257.

[72] Ko, C. K. K.; Lee, W. G. *Surf. Interface. Anal.* **2010**, *42*, 1128–1130.

[73] Al-Kharafi, F.M.; Ateya, B. G.; Abd Alla, R. M. *J. Appl. Electrochem.* **2004**, *34*, 47–53.

[74] Yazdanshenas, M. E.; Shateri-Khalilabad, M. *Journal of Industrial Textiles*. **2013**, *42*, 459–474.

[75] Hossain, M. K.; Kitahama, Y.; Huang, G. G.; Han, X.; Ozaki, Y. *Anal Bioanal Chem*. **2009**, *394*, 1747–1760.

[76] Goodall, B. *Phys. Chem. Chem. Phys.* **2012**, *15*, 1382-1388.

[77] Hu, J.; Zhao, B.; Xu, W.; Fan, Y.; Li, B.; Ozaki, Y. *Langmuir* **2002,** *18*, 6839-6844.

[78] Yuan, H.; Khoury, C. G.; Hwang, H.; Wilson, C. M.; Grant, G. A.; Vo-Dinh, T. *Nanotechnology*. **2012**, *23* (075102), 1-9.

[79] Zeman, E. J.; Schatz, G. C. *J. Phys. Chem.* **1987**, *91*, 634–643.

[80] Sharma, B. Cardinal, M. F.; Kleinman, S. L.; Greeneltch, N. G.; Frontiera, R. R.; Blaber, M. G.; Schatz, G. C.; Van Duyne, R. P. *Materials Research Society*. **2013**, *38*, 615-624.

[81] Al-Saleh, I. Abduljabbar, M.; Al-Rouqui, R.; Elkhatib, R.; Alshabbaheen, A.; Shinwari, N. *Biol Trace Elem Res*. **2013**, *153*, 145–154.

[82] Ding, G.; Han, S.; Wang, P.; Gao, Y.; Shi, R.; Wang, G.; Tian, Y. *Environmental Pollution.* **2012**, *167*, 110-114.

[83] Cai, L.; Song, X.; Zhang, W.; Luo, N.; Cai, L. *Science of the Total Environment*. **2013**, *450-451*, 266-270.

[84] Rasmussen, A.; Deckert, V. *J Raman Spectrosc*. **2006**, *37*, 311-317.

[85] Liu, D.; Wyttenbach, T.; Bowers, M. T. *J. Am. Chem. Soc.* **2006**, *128*, 15155–15163.

[86] Völkel, M.; Kiranoglu, M.; Schuster, R.; Fromme, H.; HBMnet. *Toxicology Letters*. **2014**, *225*, 222–229.

[87] Singh, S.; Srivastava, K.; Donfack, P.; Schlucker, S.; Materny, A.; Asthana, B. P. *Phys. Chem. Chem. Phys.* **2012**, *14*, 14315–14324.

[88] Otto, C.; van den Tweel, T. J. J.; de Mul, F. F. M.; Greve, J. *J. Raman Spec*. **1986**, *17*, 289-298.

[89] Giese, B.; McNaughton, D. *Biopolymers*. **2003**, *72*, 472-489.

Appendix

Table A-1. Band assignment for the normal Raman of pure powder and SERS signal of 4,4'-byp (0.1M) on a AgNP coated screen-printed electrode.

Normal Raman (cm^{-1})	**SERS (cm^{-1})**	**Assignment** [69, 70]
1620		In-plane *ν*(C-C)
1606	1603	*ν*(C-C)
1595		-
	1566	-
1510	1513	ν(C-N) and ν(C-N)
1297	1293	Ring in-plane deformation, ν(C–C), ν(C–N), δ(C–H)
1218		C-H in-plane bend (A1)
	1012	Ring in-plane deformation
999	1001	Ring breathing
	769	Ring in-plane deformation, γ(C–H), γ(C–C), γ(C–N)
674	682	Ring breathing
659		Ring breathing
574		-
385		-
318		-

ν, stretch; δ, in-plane bend; γ, out-of-plane bend

Table A-2. Band assignment for the normal Raman of metal-coated silk fabric at two excitation wavelengths.

Normal Raman (cm^{-1}) 532 nm excitation	**Normal Raman (cm-1) 780 nm excitation**	**Assignment** [72, 73]
1727	1727	-
1611	1614	Phenylalanine, tyrosine, aromatic ring stretching
	1595	Tryptophan, phenylalanine
1577		-
1483		-
1395	1395	$\delta_{as}[C(CH_3)_2]$, COO^- symmetrical stretch in aspartic and glutamic acid
1337		δCH_3
	1310	-
1290		CH_3 symmetric bending, Hα bending
	1256	Amide III random coil
1226		Amide III, alanine symmetry: N-H in-plane bending, CH_2 twisting
	1206	Tyrosine, phenylalanine
	1187	-
1169	1171	ν(C-C)
1124		-
	1114	-
	1001	Aromatic ring breathing in phenylalanine and tyrosine
949		α-Helix
885		ν(C-C), ν(C-N), ν(C=O)
816	812	-
	631	-
	514	-

ν, stretch; δ, in-plane bend

Table A-3. Band assignment for the normal Raman spectrum of pure dGMP powder.

Normal Raman (cm^{-1})		**Assignment** [87]
1722	*w*	-
1696	*w*	-
1571, 1491	*vs*	ν(C=N) and NH_2 scissoring in guanosine moiety
1477	*vs*	-
1422	*w*	-
1416	*m*	-
1361	*s*	-
1332	*s*	C-H bending in ribose ring
1211, 1183	*w*	N-H and C-H bending in guanosine moeity
1087	*w*	-
982	*s*	O-H bending of monophosphate unit
877	*m*	-
859	*m*	-
781	*w*	ν(P-O) and out-of-plane bend of ribose
680	*s*	O-H bending on phosphate, NH_2 rocking and N-H bending on guanosine ring
662	*w*	-
580	*m*	-
497	*m*	-
394	*w*	-
358	*m*	-

Figure A-4. Band assignment for the normal Raman of guanine powder.

Normal Raman (cm^{-1})		**Assignment** [88, 89]
1674	*w*	ν(C=O), ν(C=N)
1548	*m*	NH_2 scissoring, ν(C=N—C-NH_2)
1465	*w*	-
1421	*w*	-
1390	*m*	ν(C-N + C-N—C=C), C-H rocking
1359	*w*	ν(C-N—C-C)
1264	*m*	Amide III, arising from the coupling of C-N stretching and N-H bonding.
1233	*s*	ν(C=N)
1186	*w*	-
1048	*w*	ν(N-C), NH_2 rocking
936	*m*	ν(C-C backbone)
847	*w*	-
649	*vs*	Ring breathing
561	*w*	N-C=N bending
544	*w*	-
494	*w*	-
397	*w*	-

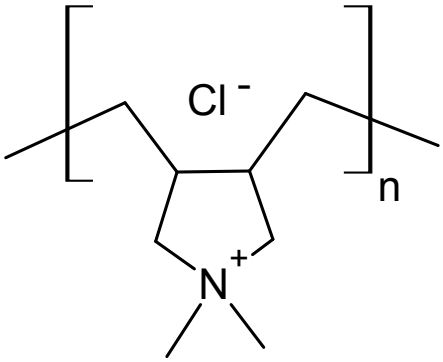

Figure A-1. Structure of polydiallyldimethylammonium chloride (PDDA), which is used as a reducing and stabilizing agent in the synthesis of TOC AuNPs.

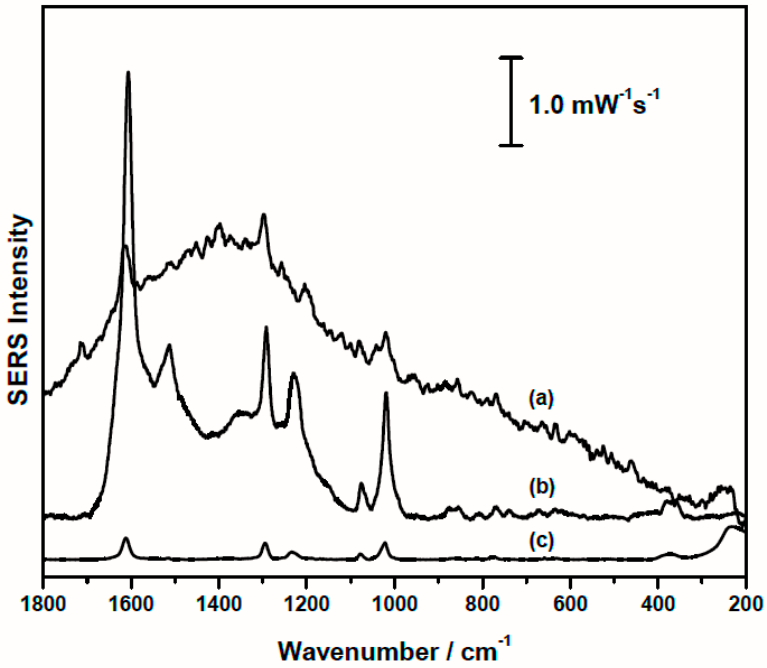

Figure A-2. SERS signal of 4,4'-byp on a fabric sample after incubation in modified citrate-reduced AgNPs, collected using a (a) 785 nm laser (55.9 mW, 30 s, signal was multiplied 5 times for an easier comparison), (b) a 532nm laser (10 mW, 60 s), and (c) a 780 nm laser (40 mW, 60 s).

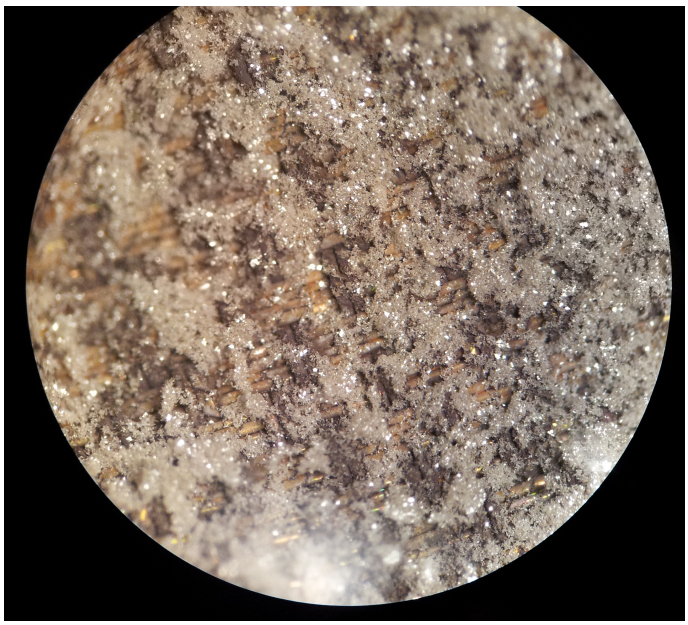

Figure A-3. Silver crystals formed on the surface of metal-coated silk fabric during *in situ* synthesis of AgNPs. Collected using a light microscope (500 x).

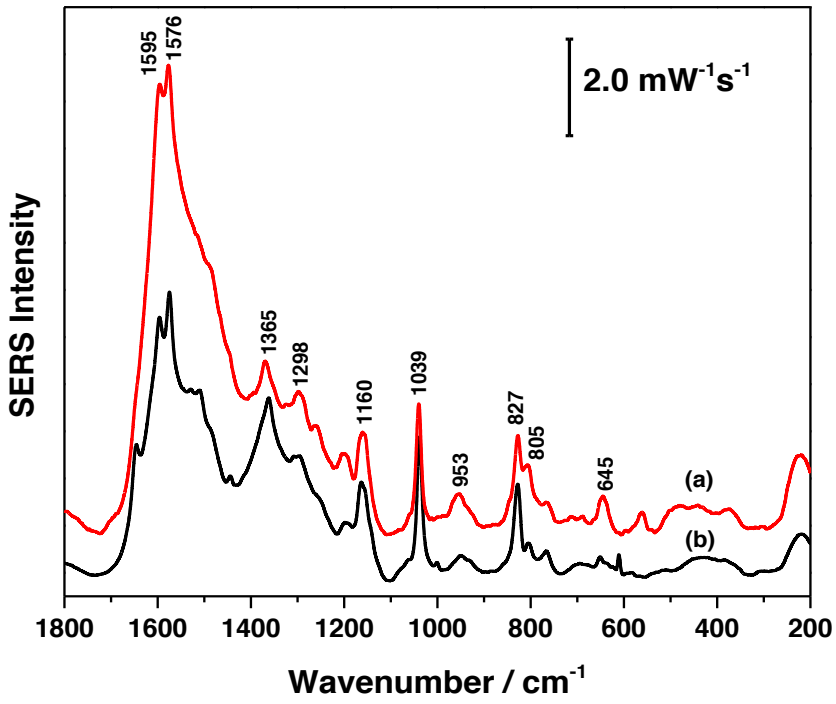

Figure A-4. SERS spectrum of fabric treated by *in situ* synthesis of Ag microspheres (a) before and (b) after deposition of dGMP solution (0.1 M). Average of 10 spectra collected at 5 mW, for 40 s, with 532 nm laser.

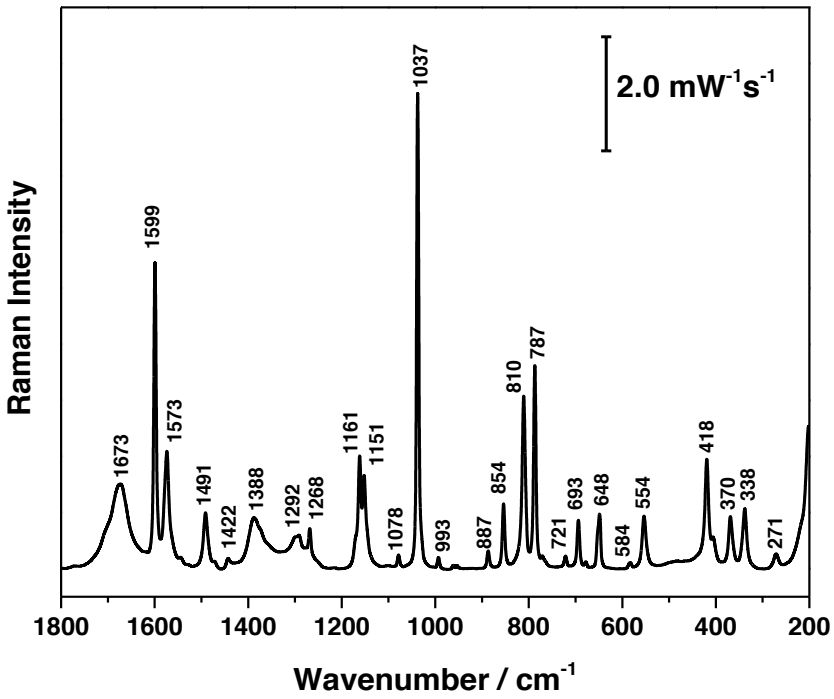

Figure A-5. Normal Raman spectrum of potassium biphthalate powder (532 nm, 10 mW, 40 s).

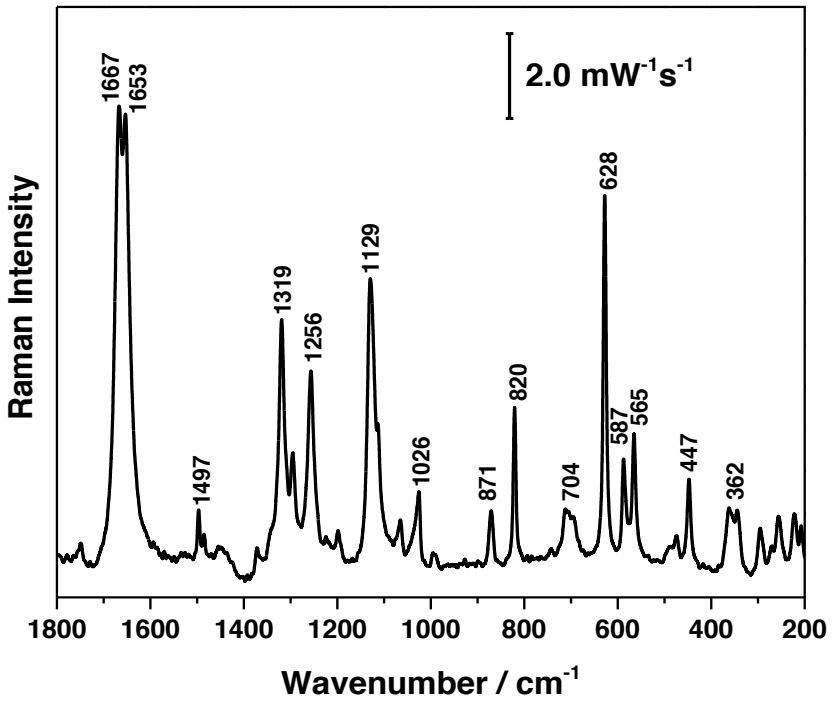

Figure A-6. Normal Raman spectrum of ascorbic acid powder (532 nm, 7 mW, 30 s).

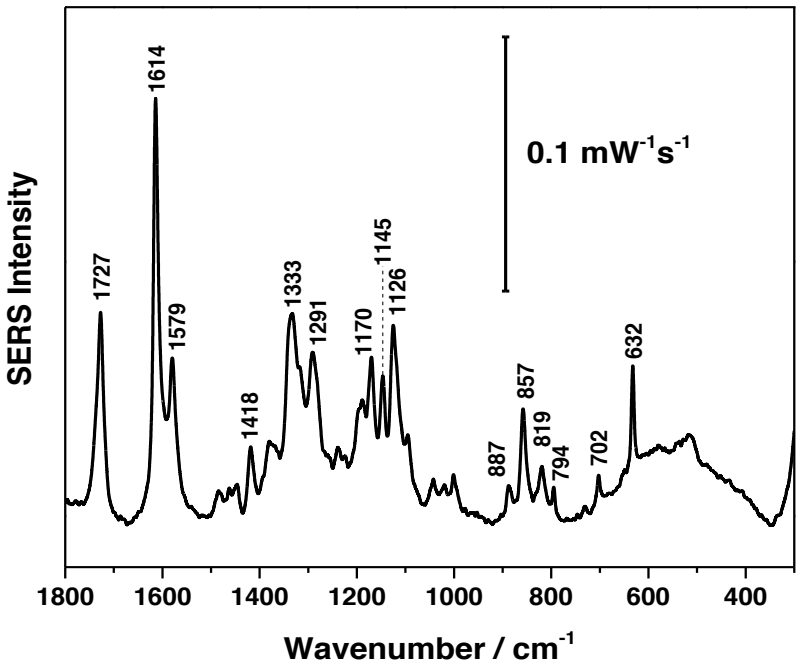

Figure A-7. SERS of dGMP on fabric incubated in concentrated AuNFs. Average of 12 spectra, collected with the 785 nm laser, at 70 mW for 30 s.

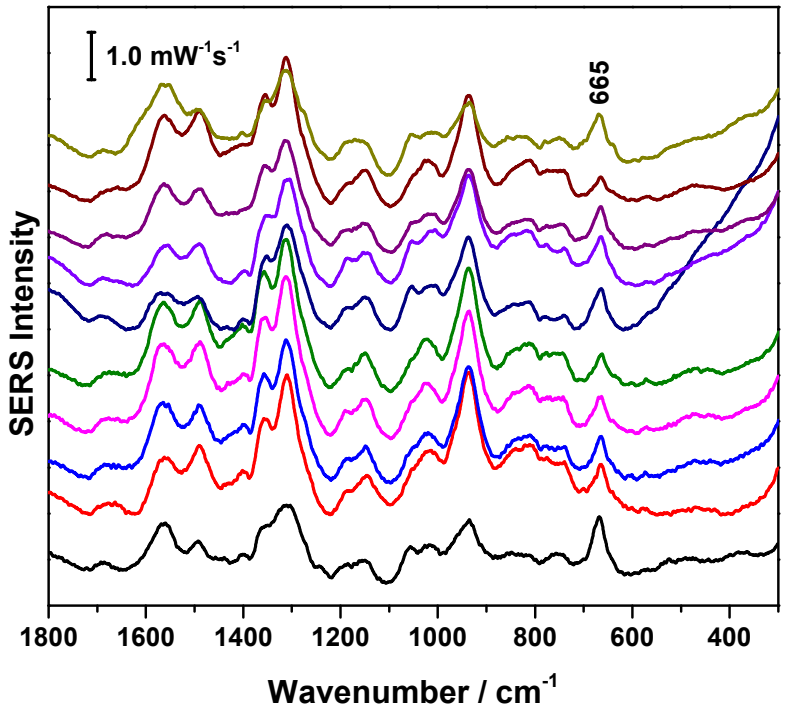

Figure A-8. SERS spectra of guanine (1.0 mM) on fabric chip treated by deposition of 20 μL of citrate-reduced AgNP paste, at 10 different spots (532 nm, 2 mW, 40 s).